Those with small deletions (patient 14) were expected to have two green and one red signal. FISH signals were counted in 205~457 nuclei of the 4 patients (including the control patient). Although six cells were obtained from patient 12, metaphase FISH was unsuccessful because of the scarcity of metaphase cells on FISH slides.

Results

Chromosome analyses

Patient data and karyotypes are summarized in Table 1. In nine patients (six MDS cases, one MPN case, one AML case, and one case of NHL in a leukemic phase), the del(20q) was the sole abnormality. Two of the five AML patients had trisomy 8, another had trisomy 1q and monosomy 7q due to a t(1;7), and one other had trisomy 1q and monosomy 16q due to a t(1;16), all in addition to the del(20q). Although the del(20q) clone was predominant in the metaphase cells of patient 12, who had WM and a B-cell–lineage malignancy, 1 of 24 cells showed a del(7q) and a normal pair of chromosomes 20 in the TPA-stimulated culture. At that time, the cell was not recognized as a clone; as the only del(7q) cell, it did not meet the criteria for a clone (12). Patient 15, who carried an inv(16) aberration at the initial stage and served as a control for FISH, was in remission and had only normal karyotypes.

Most of 20q was lost in eight cases (large deletions in patients 2, 3, 5, 7, 9, 11, 12, and 13), and one positive Q-band (q12 or q13.2) remained in six cases (small deletions in the remaining patients). However, accurate delineation was impossible using the banding technique (Table 1).

Microarray CGH analyses

We used aCGH to accurately define the breakpoints and CDR in the del(20q) cases. Figures 1 and 2 and Table 2 show the positive aCGH results of 12 patients. All of the deletions were interstitial, and both the proximal and distal breakpoints varied among patients. The centromeric breakpoints were located in the 20q11.21~12 region, and the telomeric breakpoints in the 20q13.13~13.33 region. The extent of the deletion ranged from 11.2 to 27.3 Mb. The deletion was recognized microscopically as "large" when it was greater than 18 Mb and "small" when it was less than 15 Mb. However, two patients displayed an intermediate deletion (patients 4 and 9), suggesting that the two categories provide inadequate definition in such cases. The commonly deleted region was defined as chr20:39,933,662–47,180,979, and the deletion's size was estimated to be 7.2 Mb (Table 2 and Figure 2), corresponding to chromosome bands 20q12~20q13.13. Two commonly retained regions (CRRs) were present. The one located proximal to 30,100,973 bp corresponds to chromosome bands 20q11.1~20q11.21 and is 3 Mb in length. The other is a subtelomeric CRR distal to 58,444,848 bp within band 20q13.33 and is 4 Mb in length (Table 2 and Figure 2).

Patients who demonstrated multiple clones in the chromosome analysis showed some inconsistent results regarding clone size between the karyotype and aCGH analyses. Patient 12 displayed 25 del(20q) cells (89.2%) and 3 normal cells in the overnight culture without any stimulation (Table 1). The aCGH analysis of the DNA sample from this culture revealed a predominant del(7q) clone and a del(20q) clone that was less frequent (data not shown). The del(7q) clone was detected in only one metaphase cell from the

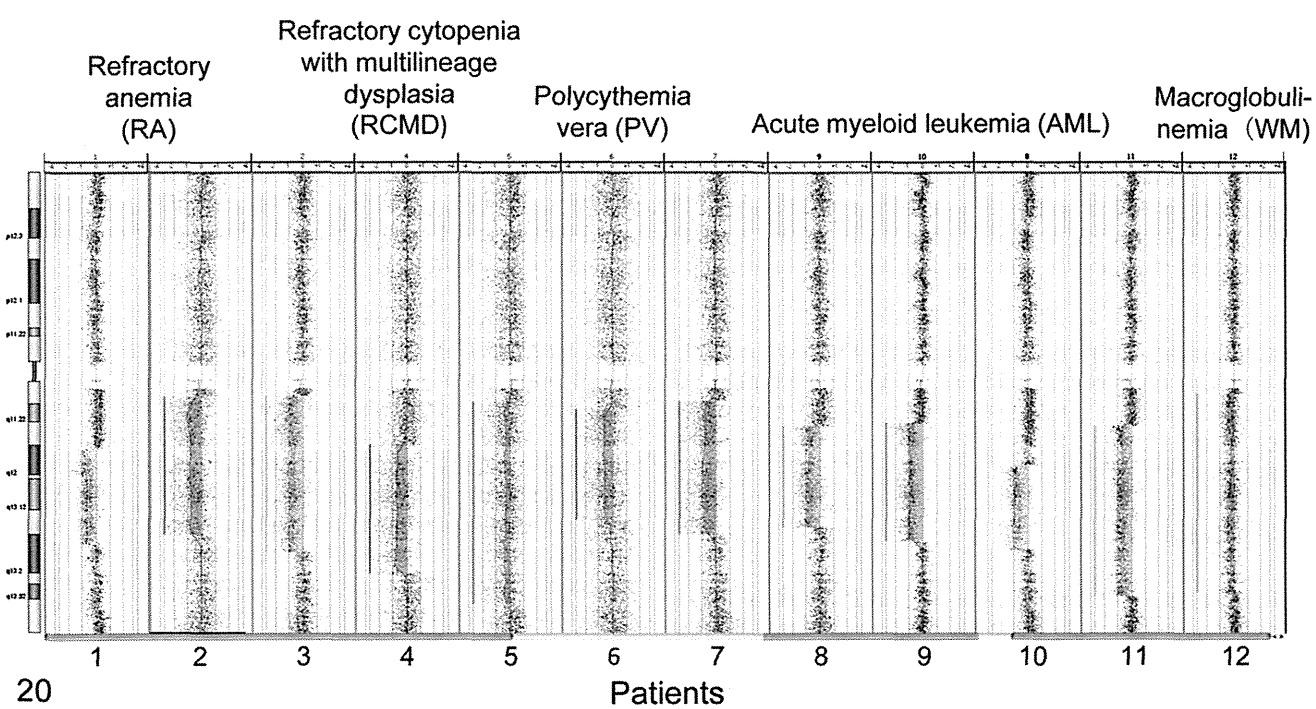

Figure 1 The results of aCGH analyses of del(20q). Patients 1–2, RA; 3–5, RCMD; 6, PV; 7–11, AML; 12, WM. Left shifts indicate the deleted segments of 20q. A slight shift was observed in two patients (patients 5 and 12), reflecting the coexistence of normal and abnormal clones in the samples.

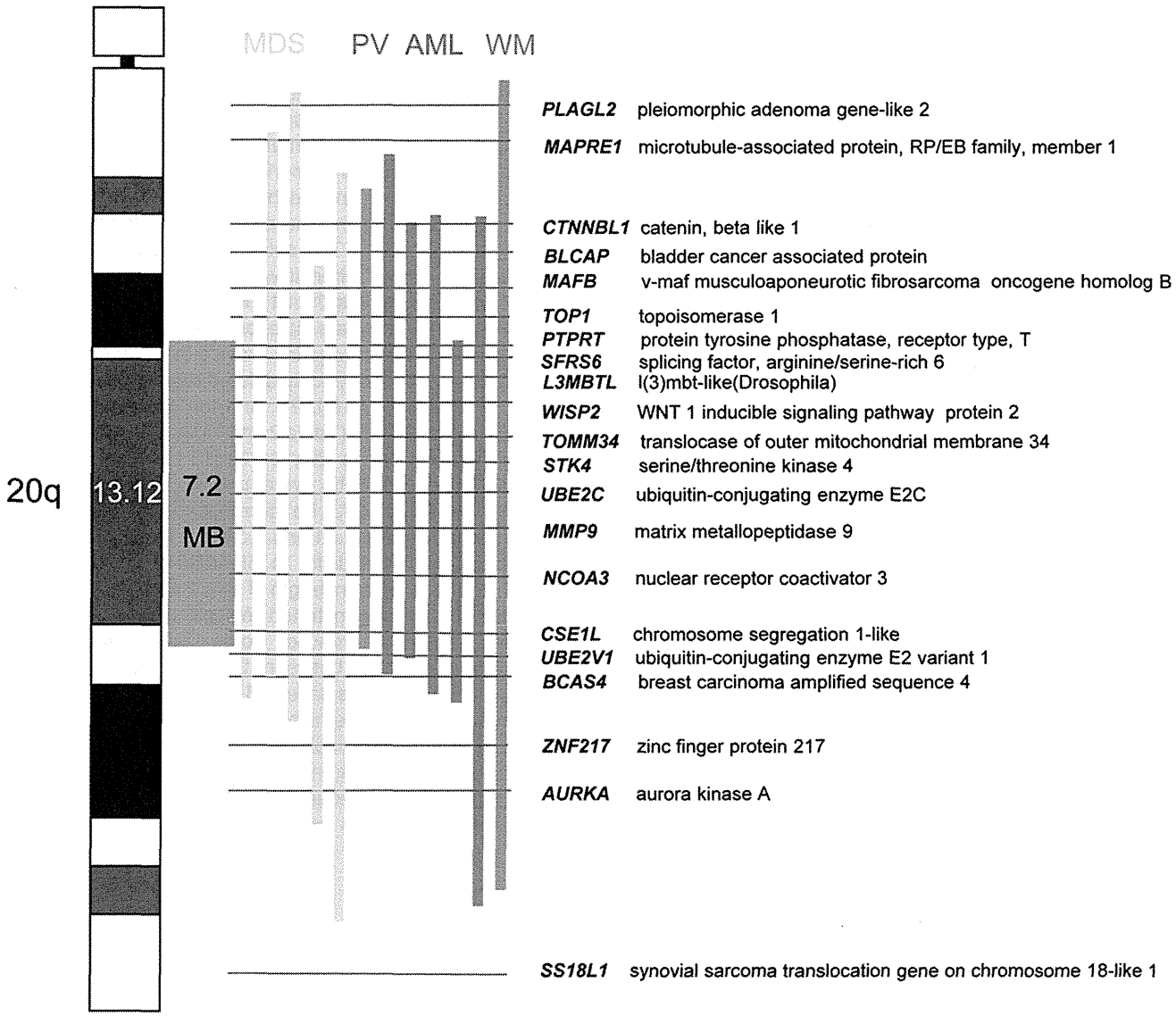

Figure 2 An ideogram of the long arm of chromosome 20. The 12 colored bars indicate the deleted regions in each patient. The bars are arranged in order of the patients' number, from patient 1 (left) to patient 12 (right). The CDR is shown by the gray rectangle. Some of the genes mapped within and around the region are listed; these genes relate to cell cycle regulation, apoptosis, transcription, or tumor development and progression based on the Human March 2006 Assembly (NCBI build 36.1, hg18).

TPA-stimulated 7-day culture (Table 1). Furthermore, the del(20q) was not detected in the aCGH analyses in patients 13 and 14, although they demonstrated a del(20q) clone in 14 of 29 (48.3%) and 9 of 26 (34.6%) of their metaphase cells, respectively (Table 1).

FISH results

The results of FISH analyses are shown in Table 3. Dual-color FISH demonstrated that del(20q) cells lost both 20q probes in patients 12 and 13, showing a large deletion. This resulted in one green and one red signal in del(20q) cells, as expected. The del(20q) cells of patient 14 demonstrated two FITC-labeled probe signals. The cells showed a pattern with two green and one red signal, corresponding to a small deletion, del(20)(q12q13.3), observed on karyotype analysis.

The frequency of del(20q) cells detected with interphase FISH was lower than that of del(20q) metaphase cells detected using karyotype analyses in the three patients. In the first karyotype analyses, the del(20q) chromosomes were detected in 89.2%, 48.2%, and 34.6% of cells in patients 12, 13, and 14, respectively, and in 80.0%, 30.0%, and 23.5% in the additional examination after a long period of cell storage (Tables 1 and 3). In the FISH experiments, the del(20q) was detected only in 22.4%, 12.9%, and 11.7% of interphase nuclei of the three patients, respectively.

Discussion

We delineated the accurate breakpoints of del(20q) chromosomes using an aCGH technique. The results show that the

deletions vary between 11.2 and 27.3 Mb rather than being classifiable into two distinct categories, large and small. The 7.2 Mb CDR ranges from the distal region of 20q12 to the proximal region of 20q13.13, the center of which contains 20q13.12 (Figure 2). The CDR of our study is more distal than any reported previously, which have ranged from 20q11.2 to 20q12~13.12 (5–7,13,14). Recently, Huh et al. (8) characterized two CDRs and two CRRs on 20q using a genomewide single nucleotide polymorphism array. They reported that CDR1 spanned 2.5 Mb between bands 20q11.23 and 20q12, whereas CDR2 encompassed 1.8 Mb within 20q13.12, CRR1 spanned 1.9 Mb within 20q11.21, and CRR2 encompassed 2.5 Mb within 20q13.33. Comparing our data with those of Huh et al. (8), our CDR (39,933,662–47,180,979 bp) does not include CDR1 (34,968,632–37,417,814 bp), and is located more distally than their regions. These differences might be partly due to the techniques used. Further studies with a larger number of patients would resolve this issue.

It has been suggested that one or more tumor suppressor genes could be located in the CDR, the deletion or inactivation of which may play a role in malignant growth (3,7,14–18). Among the genes within the CDR, *L3MBTL1* was recently reported to be a candidate tumor suppressor gene, with a proposal that the loss of the L3MBTL 1 protein contributed to the development of 20q– hematopoietic malignancies by inducing genomic instability (18). However, as so many genes lie within and around the region, it is possible that multiple genes are involved in malignant development. Genes located in the retained chromosomal regions may also be important in tumor pathogenesis, as pointed out by Douet-Guilbert et al. (7). Some of the genes relating to cell cycle regulation, apoptosis, transcription, or tumor development and progression in these regions are shown in Figure 2 based on the Human March 2006 Assembly (NCBI build 36.1, hg18). To find mutations in the candidate genes present in the CDR or CRR, studies with next-generation sequencing techniques coupled with a target enrichment system (Agilent Technologies) are now in progress, using several of the present patients. If no mutation is found, the hypothesis of haploinsufficiency of multiple genes on 20q might be considered, as supported by Huh et al. (8).

A difference in the techniques used produced some inconsistent results in clone size for patients 12, 13, and 14. Patient 12 was diagnosed with WM and showed frequent del(20q) cells in his karyotype analyses. Del(20q) is rarely reported in cases of lymphoid malignancies (2). Our aCGH analysis suggested that most cells of this patient carried a del(7q) abnormality (data not shown). We considered the possibility that the del(20q) clone comprised not lymphoid cells, but MDS cells, which demonstrated a growth advantage in vitro. However, bone marrow smears revealed that more than 90% of the cells were tumor cells, and no characteristics of MDS were found. Thus, we assumed that the del(20q) cells were lymphoid cells, although their pathogenic role was unclear. A del(20q) was not detected by aCGH in patient 13 or 14, in whom more than 30% of metaphase cells demonstrated the deletion in the first karyotype analysis (Tables 1 and 2). FISH analyses were performed to estimate the clone size of del(20q) cells in patients 12, 13, and 14 (Table 3). The frequency of del(20q) cells detected by interphase FISH was 22.4% in patient 12, 12.9% in patient 13, and 11.7% in patient 14. The results show that del(20q) cells were detected at a higher frequency in metaphase cells by karyotype analyses than in interphase nuclei using FISH. In addition, FISH patterns of del(20q) were more frequently observed in big nuclei, which were thought to be in a dividing stage, than in small, compact nuclei in a resting stage. To explain this, a few possibilities may be considered: del(20q) cells might have a growth advantage in vitro; normal lymphocytes might decrease the frequency of del(20q) because of peripheral blood contamination when the bone marrow is aspirated; or a selection bias may occur in the microscopic observations. It is possible that cell dynamics and mitotic behaviors vary among patients, and as our results are limited to only three patients, two of whom have lymphoid malignancies, further studies are needed to draw a conclusion.

As we could delineate the breakpoint of the del(20q) of patient 12 using aCGH, but not that of patient 13 or 14, the sensitivity of aCGH seems to depend on the target cell density. It is likely that target cells need to occupy more than 20% of the cell population for a successful aCGH analysis, at least within the limits for our cases. The aCGH and FISH techniques have the advantage of producing findings regarding both dividing and non-dividing cell populations. Therefore, karyotype, FISH, and aCGH analyses can complement each other in cases where multiple clones are present, such as in bone marrow aspirates.

In conclusion, we accurately delineated the breakpoints of a del(20q) in 12 patients using an aCGH analysis, which has the advantage of detecting abnormalities in non-dividing cells, although this is limited to copy number changes. The CDR found in our study is located more distally than any reported previously. Further accumulation of data is needed to resolve this discrepancy and to identify candidate pathogenic genes.

Acknowledgments

This research was supported in part by Shiseikai Corporate Juridical Person.

References

1. Greenberg P, Cox C, LeBeau MM, et al. International scoring system for evaluating prognosis in myelodysplastic syndromes. Blood 1997;89:2079–2088.
2. Mitelman F. Catalog of chromosome aberrations in cancer. New York: Wiley-Liss; 1991.
3. White NJ, Nacheva E, Asimakopoulos FA, et al. Deletion of chromosome 20q in myelodysplasia can occur in a multipotent precursor of both myeloid cells and B cells. Blood 1994;83: 2809–2816.
4. Hollings PE, Rasman I, Beard ME. A 20q deletion originating in a pluripotent stem cell. Blood 1994;83:305–306.
5. Nacheva E, Holloway T, Carter N, et al. Characterization of 20q deletions in patients with myeloproliferative disorders or myelodysplastic syndromes. Cancer Genet Cytogenet 1995;80:87–94.
6. Bench AJ, Nacheva EP, Hood TL, et al. Chromosome 20 deletions in myeloid malignancies: reduction of the common deleted region, generation of a PAC/BAC contig and identification of candidate genes. Oncogene 2000;19:3902–3913.
7. Douet-Guilbert N, Basinko A, Morel F, et al. Chromosome 20 deletions in myelodysplastic syndromes and Philadelphia-chromosome-negative myeloproliferative disorders:

characterization by molecular cytogenetics of commonly deleted and retained regions. Ann Hematol 2008;87:537–544.
8. Huh J, Tiu RV, Gondek LP, et al. Characterization of chromosome arm 20q abnormalities in myeloid malignancies using genome-wide single nucleotide polymorphism array analysis. Genes, Chromosomes & Cancer 2010;49:390–399.
9. Okada M, Hirai M, Suto Y, et al. Microarray CGH analyses of hematopoietic malignancies with chromosome 20q deletions. Advances in Chromosome Science 2009;3:164–166.
10. Vardiman JW, Thiele J, Arber DA, et al. The 2008 revision of the World Health Organization (WHO) classification of myeloid neoplasms and acute leukemia: rationale and important changes. Blood 2009;114:937–951.
11. Swerdlow SH, Campo E, Harris NL, et al. WHO classification of tumours of haematopoietic and lymphoid tissues. 4th edition. Lyon, France: IARC Press; 2008.
12. Shaffer LG, Slovak ML, Campbell LJ, editors. ISCN 2009: an international system for human cytogenetic nomenclature. Basel, Switzerland: Karger; 2009.
13. Asimakopoulos FA, White NJ, Nacheva E, et al. Molecular analysis of chromosome 20q deletions associated with myeloproliferative disorders and myelodysplastic syndromes. Blood 1994;84:3086–3094.
14. Wang PW, Eisenbart JD, Espinosa R III, et al. Refinement of the smallest commonly deleted segment of chromosome 20 in malignant myeloid diseases and development of a PAC-based physical and transcription map. Genomics 2000;67:28–39.
15. Roulston D, Espinosa R III, Stoffel M, et al. Molecular genetics of myeloid leukemia: identification of the commonly deleted segment of chromosome 20. Blood 1993;82:3424–3429.
16. Asimakopoulos FA, Gilbert JGR, Aldred MA, et al. Interstitial deletion constitutes the major mechanism for loss of heterozygosity on chromosome 20q in polycythemia vera. Blood 1996; 88:2690–2698.
17. Li J, Bench AJ, Vassiliou GS, et al. Imprinting of the human L3MBTL gene, a polycomb family member located in a region of chromosome 20 deleted in human myeloid malignancies. Proc Natl Acad Sci USA 2004;101:7341–7346.
18. Gurvich N, Perna F, Farina A, et al. L3MBTL 1 polycomb protein, a candidate tumor suppressor in del(20q12) myeloid disorders, is essential for genome stability. Proc Natl Acad Sci USA 2010; 107:22552–22557.

c-Maf plays a crucial role for the definitive erythropoiesis that accompanies erythroblastic island formation in the fetal liver

Manabu Kusakabe,[1,2] Kazuteru Hasegawa,[1] Michito Hamada,[1] Megumi Nakamura,[1] Takayuki Ohsumi,[1] Hirona Suzuki,[1] Mai Thi Nhu Tran,[3] Takashi Kudo,[1] Kazuhiko Uchida,[4] Haruhiko Ninomiya,[2] Shigeru Chiba,[2] and Satoru Takahashi[1]

[1]Department of Anatomy and Embryology, Institute of Basic Medical Sciences, and [2]Department of Hematology, Institute of Clinical Medicine, Graduate School of Comprehensive Human Sciences, University of Tsukuba, Tsukuba, Ibaraki, Japan; [3]Laboratory of Stem Cell Research and Application, University of Science, Ho Chi Minh City, Vietnam; and [4]Department of Molecular Biological Oncology, Institute of Basic Medical Sciences, Graduate School of Comprehensive Human Sciences, University of Tsukuba, Tsukuba, Ibaraki, Japan

c-Maf is one of the large Maf (musculoaponeurotic fibrosarcoma) transcription factors that belong to the activated protein-1 super family of basic leucine zipper proteins. Despite its overexpression in hematologic malignancies, the physiologic roles c-Maf plays in normal hematopoiesis have been largely unexplored. On a C57BL/6J background, *c-Maf*$^{-/-}$ embryos succumbed from severe erythropenia between embryonic day (E) 15 and E18. Flow cytometric analysis of fetal liver cells showed that the mature erythroid compartments were significantly reduced in *c-Maf*$^{-/-}$ embryos compared with *c-Maf*$^{+/+}$ littermates. Interestingly, the CFU assay indicated there was no significant difference between *c-Maf*$^{+/+}$ and *c-Maf*$^{-/-}$ fetal liver cells in erythroid colony counts. This result indicated that impaired definitive erythropoiesis in *c-Maf*$^{-/-}$ embryos is because of a non–cell-autonomous effect, suggesting a defective erythropoietic microenvironment in the fetal liver. As expected, the number of erythroblasts surrounding the macrophages in erythroblastic islands was significantly reduced in *c-Maf*$^{-/-}$ embryos. Moreover, decreased expression of VCAM-1 was observed in *c-Maf*$^{-/-}$ fetal liver macrophages. In conclusion, these results strongly suggest that c-Maf is crucial for definitive erythropoiesis in fetal liver, playing an important role in macrophages that constitute erythroblastic islands. (*Blood.* 2011;118(5): 1374-1385)

Introduction

In mouse embryogenesis, red blood cells are produced in the yolk sac in a process called primitive erythropoiesis. Erythropoiesis then takes place in the fetal liver around embryonic day (E) 10 onward and in BM and spleen after birth. This process, which is characterized by enucleated red blood cells, is called definitive erythropoiesis.[1] During terminal erythroid differentiation, erythroblasts are associated with a central macrophage, which forms a specialized microenvironment, the so-called erythroblastic islands. In the erythroblastic islands, a central macrophage provides favorable proliferative and survival signals to the surrounding erythroblasts, and it eventually engulfs the extruded nuclei of maturing erythrocytes.[2-5] Inhibition of the interaction between macrophage and erythroblasts usually leads to embryonic anemia accompanied by accelerated apoptosis of erythroid cells. Targeted disruption of the gene *palld*, which encodes actin cytoskeleton associated protein (palladin) prevented effective erythroblast-macrophage interactions because of differentiation defects in the macrophage. Therefore, mouse embryos homozygous for the mutant gene experience severe anemia and succumb in the embryonic period.[6] Meanwhile, it has been reported that a series of adhesion molecules are also involved in the process of forming erythroblastic islands. Erythroblast macrophage protein (EMP) is a transmembrane protein expressed in both erythroblasts and macrophages, and it mediates the erythroblast-macrophage interaction. Indeed, the targeted deletion of EMP causes lethal anemia in mouse embryos because of the suppressed formation of erythroblastic islands.[7] Furthermore, a previous report showed that the interaction between very late Ag-4 ($\alpha_4\beta_1$ integrin) on erythroblasts and VCAM-1 on macrophages plays a key role in maintaining the islands.[8] For example, administration of Abs raised against either $\alpha_4\beta_1$ integrin or VCAM-1 caused disruption of the island structure.[8] However, the molecular mechanism, in terms of transcriptional regulation of island-affiliated genes in macrophages, remains largely unknown.

The large Maf transcription factor c-Maf is a cellular homolog of v-maf, which was isolated from a chicken musculoaponeurotic fibrosarcoma induced by avian retrovirus AS42 infection.[9] The large Maf transcription factors contain an acidic domain that promotes transcriptional regulation and a basic region/leucine zipper domain that mediates dimerization, as well as DNA binding to either Maf recognition elements (MAREs) or the 5′ AT-rich half-MARE.[10-12] Each large Maf protein has been shown to play a distinct role in cellular proliferation and differentiation in both pathologic and physiologic situations.[9,13-19] In B-lymphoid and T-lymphoid lineages, aberrant expression of c-Maf works as an oncogene, as shown in patients with multiple myeloma and angioimmunoblastic T-cell lymphoma and in a transgenic mouse model.[20-23] Physiologic c-Maf expression is indispensable for the proper regulation of IL-4 and IL-21 gene expression in T-helper cells.[24,25] In macrophages, c-Maf has been reported to regulate IL-10 expression, which is essential for differentiation of regulatory T cells.[26] In addition, combined deficiency of MafB and c-Maf

Submitted August 4, 2010; accepted May 3, 2011. Prepublished online as *Blood* First Edition paper, May 31, 2011; DOI 10.1182/blood-2010-08-300400.

An Inside *Blood* analysis of this article appears at the front of this issue.

The online version of the article contains a data supplement.

The publication costs of this article were defrayed in part by page charge payment. Therefore, and solely to indicate this fact, this article is hereby marked "advertisement" in accordance with 18 USC section 1734.

enables long-term expansion of differentiated, mature macrophages.[27] We recently reported that c-Maf is abundantly expressed in fetal liver macrophages and that it regulates expression of F4/80, which mediates immune tolerance.[28] However, the physiologic consequences of c-Maf deletion on terminal erythroid differentiation in erythroblastic islands have been largely unexplored.

In the present study, we demonstrate that *c-Maf*–deficient mice exhibit embryonic anemia, which is associated with a failure to retain erythroblastic islands. Moreover, we found significantly reduced expression of VCAM-1 in *c-Maf*–deficient macrophages, which presumably accounts for the deficiency in island maintenance and subsequent embryonic anemia. Thus, these results suggest that c-Maf is indispensable for definitive erythropoiesis in fetal liver, because it activates VCAM-1 expression in macrophages, and this causes the maintenance of erythroblastic islands.

Methods

Mice

c-Maf–deficient mice were originally generated on a 129/Sv background[14] and have been backcrossed onto a C57BL/6J background for > 7 generations. In staging the embryos, gestational day 0.5 (E0.5) was defined as noon of the day a vaginal plug was found after overnight mating. Mice were maintained in specific pathogen-free conditions in a Laboratory Animal Resource Center. All experiments were performed according to the Guide for the Care and Use of Laboratory Animals at the University of Tsukuba.

Hematologic analysis of fetal liver cells, embryonic blood, and adult blood

Single-cell suspensions prepared from fetal livers were washed and resuspended in 1 mL of 2% FBS/PBS. The cell number was counted with the use of a hemocytometer. Collection of embryonic peripheral blood was performed as described previously.[29] Peripheral blood samples from adult mice were obtained from retro-orbital venous plexus with the use of heparin-coated microtubes. Blood counts were determined with an automated hemocytometer (Nihon Kohden). Blood smears were prepared with the wedge technique and were stained with May-Grünwald-Giemsa and then photographed with a Keyence Biorevo BZ-9000 microscope. Images were processed with Photoshop software (Adobe).

Flow cytometry

Freshly isolated fetal liver cells were immunostained at 4°C in PBS/2% FBS in the presence of 5% mouse serum to block Fc receptors. Cells were incubated with FITC-conjugated anti–TER-119 and allophycocyanin (APC)–conjugated anti-CD44 Abs, followed by a 5-minute incubation with phycoerythrin PE-conjugated Annexin V (BioVision) at room temperature. To quantify the presence of VCAM-1 and integrin αV on macrophages, FITC-conjugated anti–Mac-1, Alexa Fluor 647–conjugated anti–VCAM-1 and PE-conjugated anti-integrin αV Abs were used for analyses. All Abs except PE-conjugated annexin V were from eBioscience. Flow cytometry was performed on a Becton Dickinson FACS LSR with CellQuest software. The isolation of erythroblasts at different stages of maturation was performed as described previously.[30] Data were analyzed with FlowJo (Tree Star Inc) analysis software.

Cell cycle analysis

Cell cycle analysis was performed with propidium iodide (PI). Further details are provided in supplemental Methods (available on the *Blood* website; see the Supplemental Materials link at the top of the online article).

Histology and TUNEL assay

Whole E13.5 embryos were fixed in 10% formalin neutral buffer solution (Wako). Paraffin-embedded tissue was sectioned, mounted, and stained with H&E. TUNEL assays were performed with an in situ Apoptosis Detection Kit according to the manufacturer's protocol (TaKaRa). Images were captured by a digital camera system with the use of a Leica DM RXA2 microscope (Leica Microsystems).

CFU assay

CFU assays were performed in MethoCult GF M3434 (StemCell Technologies) for erythroid burst-forming unit (BFU-E) and granulocyte, erythroid, megakaryocyte, and macrophage CFU (CFU-GEMM), and M3334 for erythroid CFU (CFU-E), following the manufacturer's instructions. CFU-E was scored 2 days after plating. BFU-E and CFU-GEMM were scored 8 days after plating.

Preparation of "native" erythroblastic islands and "reconstituted" erythroblastic islands

Native erythroblastic islands were isolated from fetal livers with the use of a previously described protocol.[31] Full details are provided in supplemental Methods.

Microarray analysis of fetal liver macrophages

Microarray analysis was performed as described previously.[32] Further details are provided in supplemental Methods. The data have been deposited in the Gene Expression Omnibus database under the accession number GSE23305.

Real-time RT-PCR analysis of fetal liver macrophages

Macrophages were prepared from fetal livers of *c-Maf*$^{+/+}$ or *c-Maf*$^{-/-}$ mice. Separation of fetal liver macrophages with the use of Mac-1^{+} magnetic beads and the MACS system was performed as described previously.[28] RNA extraction and quantitative RT-PCR were performed as described previously.[28] Primers used for PCR and the PCR conditions are available in supplemental Table 1.

Luciferase reporter assay

The *VCAM-1* 0.7 kilobase (kb) promoter (VCAM-1 Luc) or VCAM-1 mut Luc ligated to a luciferase reporter[33] was transiently cotransfected with c-Maf expression plasmids in macrophage cell line J774 with the use of FuGENE 6 (Roche). Twenty-four hours after the transfection, cells were collected, and reporter gene assays were performed with the Dual Luciferase Kit (Promega). Transfection efficiency was normalized to the expression of *Renilla* luciferase.

Reconstitution of hematopoietic system with fetal liver cells

The donor cells for hematopoietic reconstitution were prepared from E14.5 fetal livers of *c-Maf*$^{+/+}$ or *c-Maf*$^{-/-}$ (C57BL/6J-Ly5.1) mice. Fetal liver cells (2×10^6 cells) were injected into the tail vein of 8- to 10-week-old C57BL/6J-Ly5.2 mice that were previously exposed to x-rays at a 10-Gy dose.

Phenylhydrazine stress test

Mice were injected subcutaneously on days 0, 1, and 3 with 50 mg/kg phenylhydrazine (PHZ) hydrochloride solution in PBS as previously described.[34] Blood was obtained from the retro-orbital plexus on days 0, 3, 6, 8, and 10.

Statistical analysis

Data were represented as mean ± SEM. Statistical significance between any 2 groups was determined by the 2-tailed Student *t* test, in which *P* values < .05 were considered significant.

Table 1. Genotypic analysis of neonates and embryos from *c-Maf*$^{+/-}$ intercross on a C57BL/6J background

Embryonic stage	No. of each *c-Maf* genotype (no. of dead embryos)			Total no. of embryos
	c-Maf$^{+/+}$	*c-Maf*$^{+/-}$	*c-Maf*$^{-/-}$	
E12.5	13	30	15	58
E13.5	57	88	46 (5)	191
E14.5	75	135	55 (12)	265
E15.5	35	58	16 (3)	109
E16.5	11	15	4 (3)	30
E18.5	14	18	4 (3)	36
Neonate	13	29	0	42

Embryos were isolated at the indicated time points of gestation and within 7 days of birth (postnatal), and analyzed for viability. Genotypes of embryos were determined by PCR.

Results

Lethal erythropoietic deficiency in *c-Maf*$^{-/-}$ embryos

The *c-Maf*$^{-/-}$ mice, as originally generated, exhibited perinatal mortality within a few hours after birth on a 129/Sv background.[14] However, unexpectedly, on a C57BL/6J genetic background, c-Maf deficiency resulted in embryonic lethality from E15.5 onward, and almost all *c-Maf*$^{-/-}$ embryos died before E18.5 (Table 1). The fetal livers from *c-Maf*$^{-/-}$ embryos at E13.5 appeared pale compared with those from healthy *c-Maf*$^{+/+}$ control embryos (Figure 1A). As expected, the hematocrits of peripheral blood in the *c-Maf*$^{-/-}$ embryos (E13.5~E15.5) were markedly reduced (E13.5. 13.4% ± 1.8%; E14.5, 14.5% ± 1.0%; E15.5, 16.9% ± 1.0%), compared with the *c-Maf*$^{+/+}$ controls (E13.5, 18.7% ± 0.6%; E14.5, 23.1% ± 1.7%; E15.5, 29.6% ± 1.8%; Figure 1B). May-Grünwald-Giemsa staining of peripheral blood smears showed a significant reduction of enucleated red blood cells in *c-Maf*$^{-/-}$ embryos (E13.5, 6.68% ± 1.0%; E14.5, 17.2% ± 1.9%; E15.5, 29.8% ± 5.6%; Figure 1C-D), whereas *c-Maf*$^{+/+}$ control embryos retained a normal population of enucleated red blood cells (E13.5, 25.5% ± 4.7%; E14.5, 54.1% ± 1.1%; E15.5, 86.9% ± 2.8%; Figure 1C-D). Considering that the enucleated red blood cells are mainly derived from definitive erythropoiesis, these data suggest that c-Maf–deficient embryos suffer from impaired definitive erythropoiesis on the C57BL/6J genetic background. A previous study showed that placental insufficiency causes embryonic lethality.[35] To assess the effect of c-Maf on the placenta, immunofluorescence staining of placenta was performed with an anti–c-Maf Ab (supplemental Figure 1B). The expression of c-Maf was not detected in placenta. Compared with the head tissue as a positive control, c-Maf mRNA expression was 5-fold less in the placenta (supplemental Figure 1C). In addition, no obvious abnormalities in the *c-Maf*$^{-/-}$ placenta were observed after H&E staining (supplemental Figure 1D).

Increased apoptotic cell death in *c-Maf*$^{-/-}$ fetal liver

We next examined the cellular viability, as well as the cell cycle status, of *c-Maf*$^{-/-}$ fetal liver cells, in the hope of elucidating the molecular and cellular basis of their erythropoietic deficiency. The fetal liver size in *c-Maf*$^{-/-}$ embryos was smaller; thus, consistently fewer fetal liver cells were harvested from *c-Maf*$^{-/-}$ embryos between E13.5 and E15.5 (E13.5, 3.37 ± 0.5 × 10^6 cells; E14.5, 7.61 ± 1.0 × 10^6 cells; E15.5, 6.54 ± 2.7 × 10^6 cells) than from age-matched *c-Maf*$^{+/+}$ control embryos (E13.5, 6.89 ± 0.4 × 10^6 cells; E14.5, 16.6 ± 2.3 × 10^6 cells; E15.5, 32.5 ± 2.4 × 10^6 cells; Figure 2A-B). Of note, H&E staining of E13.5 *c-Maf*$^{-/-}$ fetal liver sections showed an increased number of pyknotic nuclei, which are indicative of apoptosis, compared with the *c-Maf*$^{+/-}$ control embryo (Figure 2C). In addition, TUNEL-positive apoptotic cells were remarkably increased in E13.5 *c-Maf*$^{-/-}$ fetal liver sections (Figure 2C). Moreover, flow cytometric analysis of PI-stained fetal liver cells showed an increased abundance of a sub-G_0/G_1 population early apoptotic cell fraction in *c-Maf*$^{-/-}$ fetal liver (8.77% ± 2.5%) compared with *c-Maf*$^{+/+}$

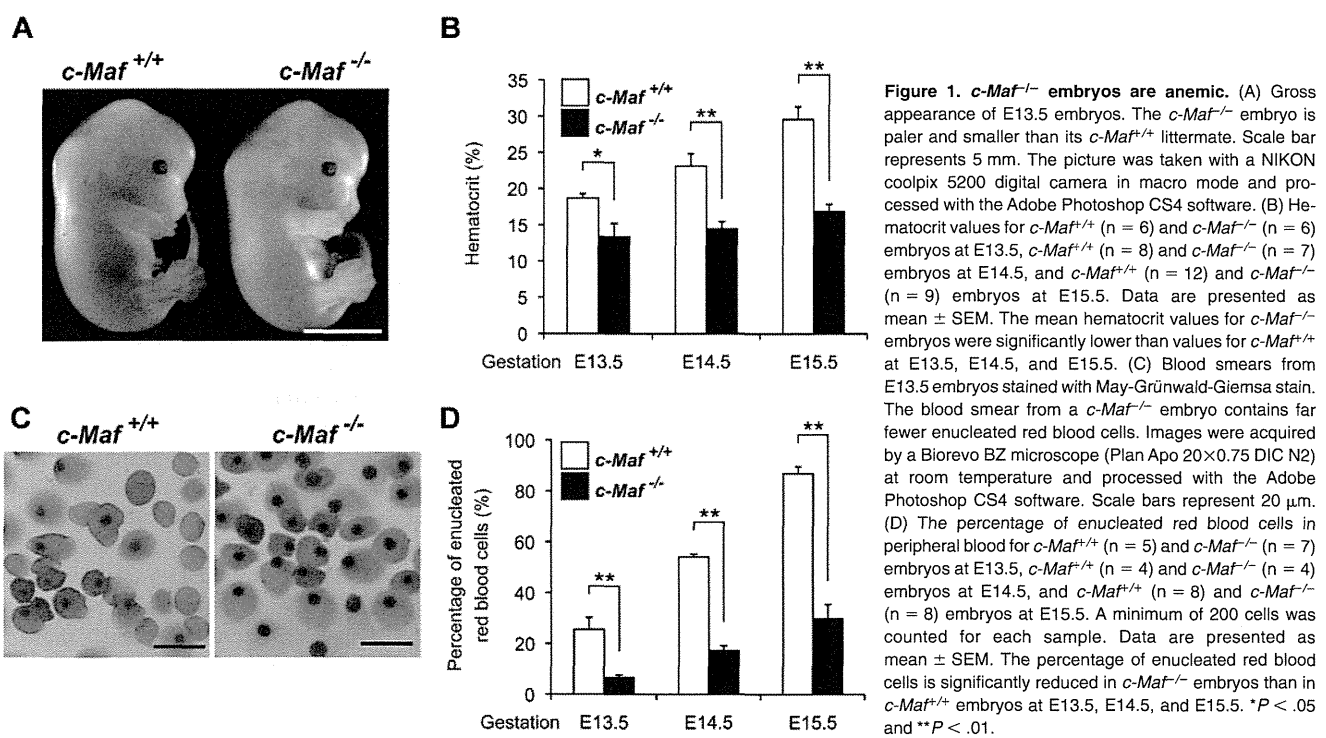

Figure 1. *c-Maf*$^{-/-}$ embryos are anemic. (A) Gross appearance of E13.5 embryos. The *c-Maf*$^{-/-}$ embryo is paler and smaller than its *c-Maf*$^{+/+}$ littermate. Scale bar represents 5 mm. The picture was taken with a NIKON coolpix 5200 digital camera in macro mode and processed with the Adobe Photoshop CS4 software. (B) Hematocrit values for *c-Maf*$^{+/+}$ (n = 6) and *c-Maf*$^{-/-}$ (n = 6) embryos at E13.5, *c-Maf*$^{+/+}$ (n = 8) and *c-Maf*$^{-/-}$ (n = 7) embryos at E14.5, and *c-Maf*$^{+/+}$ (n = 12) and *c-Maf*$^{-/-}$ (n = 9) embryos at E15.5. Data are presented as mean ± SEM. The mean hematocrit values for *c-Maf*$^{-/-}$ embryos were significantly lower than values for *c-Maf*$^{+/+}$ at E13.5, E14.5, and E15.5. (C) Blood smears from E13.5 embryos stained with May-Grünwald-Giemsa stain. The blood smear from a *c-Maf*$^{-/-}$ embryo contains far fewer enucleated red blood cells. Images were acquired by a Biorevo BZ microscope (Plan Apo 20×0.75 DIC N2) at room temperature and processed with the Adobe Photoshop CS4 software. Scale bars represent 20 μm. (D) The percentage of enucleated red blood cells in peripheral blood for *c-Maf*$^{+/+}$ (n = 5) and *c-Maf*$^{-/-}$ (n = 7) embryos at E13.5, *c-Maf*$^{+/+}$ (n = 4) and *c-Maf*$^{-/-}$ (n = 4) embryos at E14.5, and *c-Maf*$^{+/+}$ (n = 8) and *c-Maf*$^{-/-}$ (n = 8) embryos at E15.5. A minimum of 200 cells was counted for each sample. Data are presented as mean ± SEM. The percentage of enucleated red blood cells is significantly reduced in *c-Maf*$^{-/-}$ embryos than in *c-Maf*$^{+/+}$ embryos at E13.5, E14.5, and E15.5. *$P < .05$ and **$P < .01$.

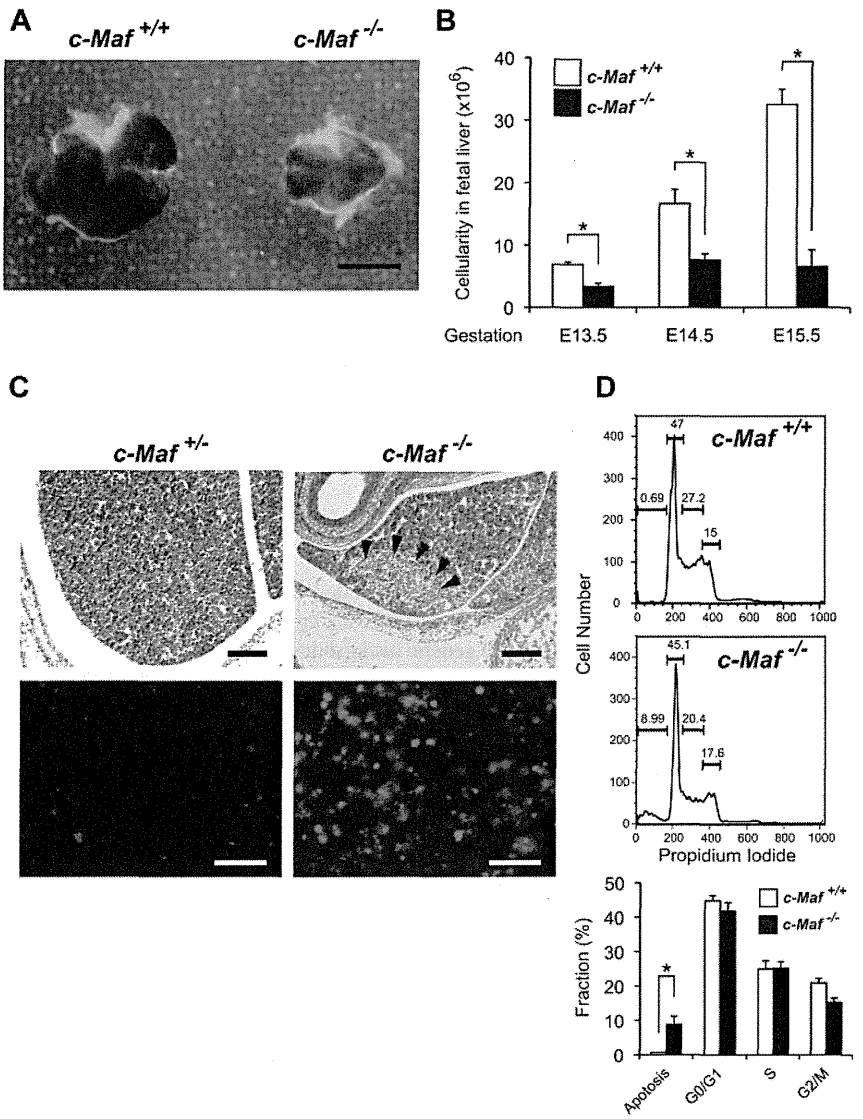

Figure 2. Increased number of apoptotic cells is observed in *c-Maf*$^{-/-}$ fetal liver. (A) Gross appearance of E13.5 fetal liver. The *c-Maf*$^{-/-}$ fetal liver is smaller than a *c-Maf*$^{+/+}$ fetal liver. Scale bar represents 100 μm. The picture was taken with a NIKON coolpix 5200 digital camera in macro mode and processed with the Adobe Photoshop CS4 software.(B) The mean total number of fetal liver cells in *c-Maf*$^{+/+}$ (n = 14) and *c-Maf*$^{-/-}$ (n = 10) embryos at E13.5, *c-Maf*$^{+/+}$ (n = 6) and *c-Maf*$^{-/-}$ (n = 4) embryos at E14.5, and *c-Maf*$^{+/+}$ (n = 8) and *c-Maf*$^{-/-}$ (n = 8) embryos at E15.5. The mean number of fetal liver cells is significantly reduced in *c-Maf*$^{-/-}$ embryos. Data are presented as mean ± SEM. (C) H&D staining of *c-Maf*$^{+/-}$ and *c-Maf*$^{-/-}$ fetal liver sections (top). Arrowheads indicate pyknotic nuclei, which indicate apoptotic cells. TUNEL assays showed increased apoptosis in the *c-Maf*$^{-/-}$ fetal liver (bottom panel). Images were acquired by a Leica DM RXA2 microscope (Lecia HC PL Fluotar 20×/0.50 PH2) at room temperature and processed with the Adobe Photoshop CS4 software. Scale bars in the top panel represent 200 μm. Scale bars in the bottom panel represent 50 μm. (D) The fraction of cells in different phases of the cell cycle was measured by PI staining followed by flow cytometric analyses. The percentage of cells in sub-G_0/G_1, G_1, S phase, and G_2/M are indicated. The sub-G_0/G_1 phase represents the apoptotic population. The apoptotic population was increased in *c-Maf*$^{-/-}$ fetal liver.

control cells (0.67% ± 0.01%; Figure 2D). However, the cellular population of each phase of the cell cycle, that is, G_0/G_1, S, and G_2/M, was not significantly affected (Figure 2D). Overall, these observations suggest that the fetal liver hematopoietic cells from *c-Maf*$^{-/-}$ embryos are prone to undergo apoptotic cell death.

Impaired fetal liver erythropoiesis because of a non–cell-autonomous effect of c-Maf deficiency

Given the significant disturbance of erythropoiesis, we next attempted to delineate the maturation status of erythroid lineage cells in *c-Maf*$^{-/-}$ fetal liver. To this end, we examined fetal liver erythropoiesis by flow cytometry with the use of the erythroid markers CD44 and TER-119, which distinguish various stages of erythroid-cell differentiation (Figure 3A). By modifying a method reported by Chen et al[30] to isolate erythroblasts at different maturation stages from adult BM, we isolated erythroblasts from fetal liver cells and analyzed their structure (Figure 3B). Decreased numbers of mature erythroid compartments (regions II, III, IV, and V in Figure 3C) were observed in *c-Maf*$^{-/-}$ fetal liver than in *c-Maf*$^{+/+}$ fetal liver. These results showed a reduction of basophilic erythroblasts, polychromatic erythroblasts, orthochromatic erythroblasts, reticulocytes, and mature red cells in *c-Maf*$^{-/-}$ fetal liver. Previously, Zhang et al[36] reported a method to study erythropoiesis with the use of an anti-CD71 Ab and an anti–TER-119 Ab. Similar results were obtained with their method. Decreased numbers of mature erythroid compartments (region 3 to region 5 in supplemental Figure 2A-B) were observed in *c-Maf*$^{-/-}$ fetal liver in combination with anti-CD71 Ab and anti–TER-119 Ab. These observations prompted us to quantify the apoptotic cell population at each stage of erythroid cells by annexin V staining.

In good agreement with the preferential decrease of the mature erythroid compartments (regions II-V), we observed a highly increased number of annexin V-positive cells in the most mature erythroid compartment (region V) of *c-Maf*$^{-/-}$ fetal liver compared with the *c-Maf*$^{+/+}$ fetal liver. In contrast, the premature erythroid compartments (regions I-IV) of *c-Maf*$^{-/-}$ fetal liver cells exhibited a comparable number of annexin V-positive cells with the *c-Maf*$^{+/+}$ control (Figure 3D; supplemental Figure 2C). To examine the state of globin regulation, the Mac-1$^-$ cells from E13.5 fetal liver were sorted and analyzed for mRNA of Hbb (hemoglobin beta chain) genes by real-time RT-PCR analysis. Expression profiles showing switching of Hbb genes indicated that the definitive Hbb gene Hbb-b1 (hemoglobin, beta adult major chain) was significantly down-regulated, whereas the primitive globin genes Hbb-bH1

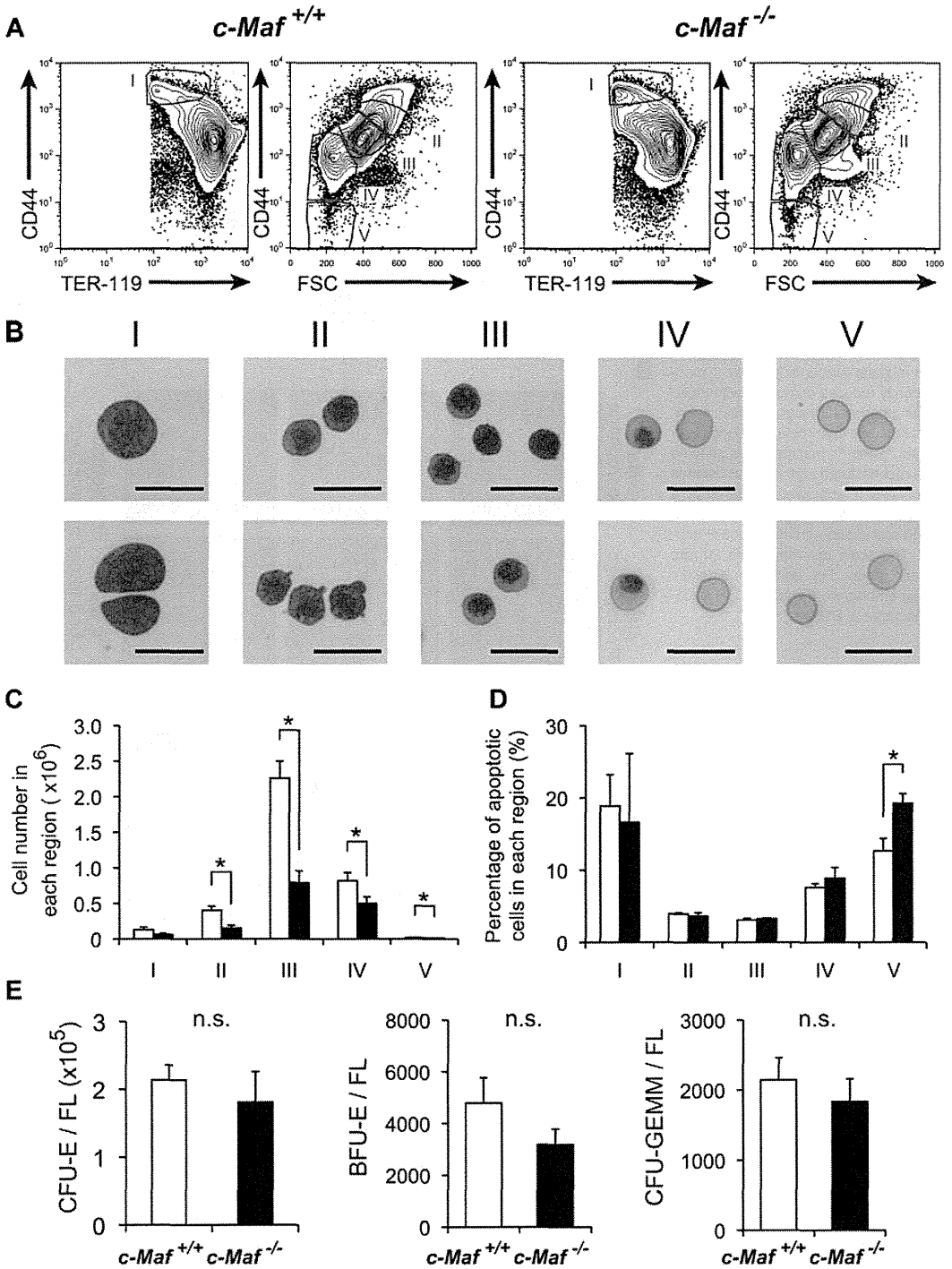

Figure 3. Definitive erythropoiesis in fetal liver is impaired in *c-Maf*$^{-/-}$ embryos but *c-Maf*$^{-/-}$ fetal liver cells can form erythroid colonies. (A) Flow cytometric analysis of fetal liver cells isolated from E13.5 embryos labeled with a FITC-conjugated anti–TER-119 mAb and an APC-conjugated anti-CD44 mAb. Regions I to V are defined by a characteristic staining pattern and forward scatter (FSC) intensity of cells as indicated. (B) Representative images of erythroblast structure on stained cytospins from the 5 distinct regions shown in Figure 3A of wild-type fetal liver. Images were acquired by a Biorevo BZ microscope (Plan Apo 20×0.75 DIC N2) at room temperature and processed with the Adobe Photoshop CS4 software. Scale bar represents 20 μm. (C) Comparison of *c-Maf*$^{+/+}$ and *c-Maf*$^{-/-}$ fetal livers in region I to region V. □ represents *c-Maf*$^{+/+}$; ■, *c-Maf*$^{-/-}$; n = 8~10 per group; $^*P < .05$. (D) The ratio of annexin V$^+$ cells from region I to region V was compared in *c-Maf*$^{+/+}$ and *c-Maf*$^{-/-}$ fetal livers. □ represents *c-Maf*$^{+/+}$; ■, *c-Maf*$^{-/-}$; n = 3 per group; $^*P < .05$. (E) In vitro colony assay with the use of fetal liver cells from *c-Maf*$^{+/+}$ (□) and *c-Maf*$^{-/-}$ (■) embryos at E13.5. A total of 20 000 fetal liver cells were plated and cultured with methylcellulose media. The numbers of CFU-E–, BFU-E–, and CFU-GEMM–derived colonies per fetal liver are shown. No significant difference (n.s.) was found in the number of CFU-E–, BFU-E–, or CFU-GEMM–derived colonies per fetal liver in *c-Maf*$^{+/+}$ embryos and *c-Maf*$^{-/-}$ embryos; n = 6~7 per group; data are presented as mean ± SEM. FL indicates fetal liver.

(hemoglobin z, beta-like embryonic chain) and Hbb-y (hemoglobin y, beta-like embroyonic chain) were not significantly suppressed in the *c-Maf*$^{-/-}$ fetal liver erythroid fraction compared with the *c-Maf*$^{+/+}$ control (supplemental Figure 3).

To examine the colony formation potential of hematopoietic progenitors in *c-Maf*$^{-/-}$ fetal liver, conventional set of CFU assays were performed. As a result of CFU assays, there were no significant differences between *c-Maf*$^{+/+}$ and *c-Maf*$^{-/-}$ in the

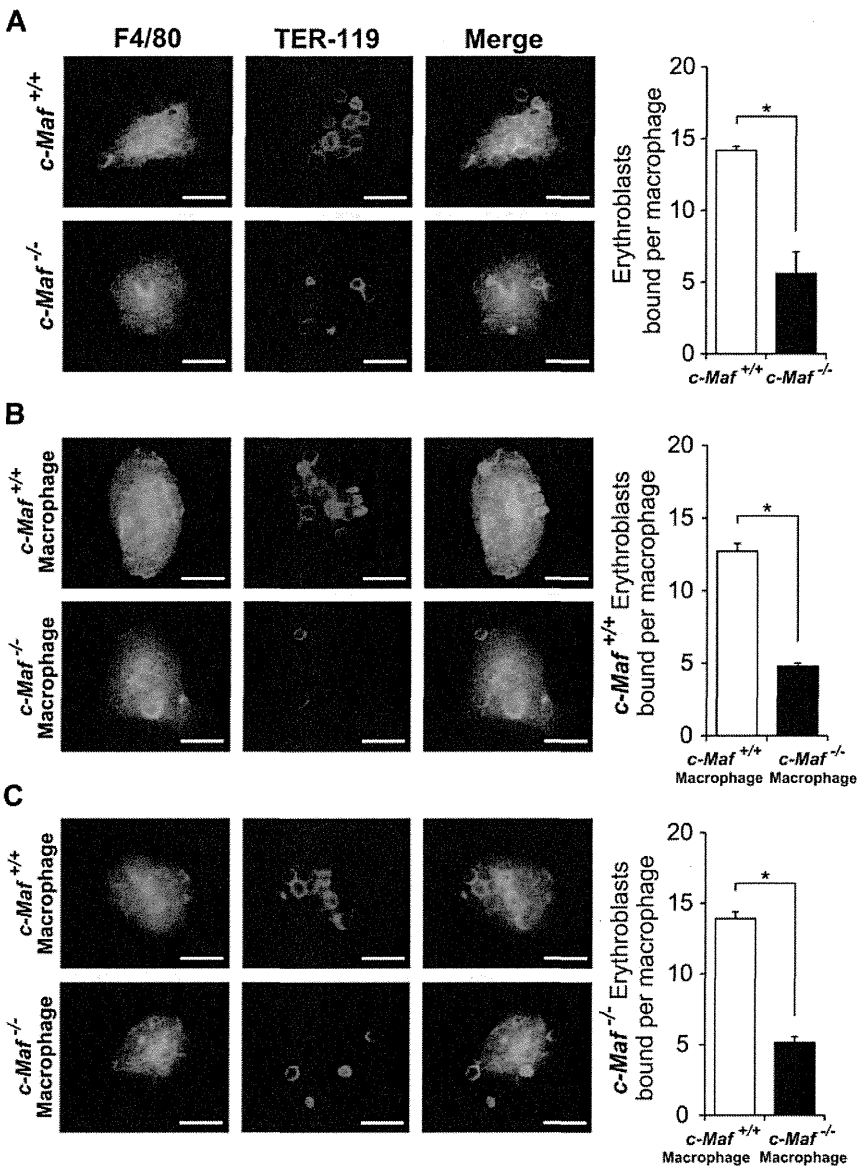

Figure 4. Absence of c-Maf impairs the formation of erythroblastic islands in the fetal liver. (A) Native erythroblastic islands isolated from *c-Maf*$^{+/+}$ and *c-Maf*$^{-/-}$ fetal liver were immunostained with F4/80 (green) and TER-119 (red) Abs as described in "Methods." F4/80 is used as a macrophage-specific marker, and TER-119 is used as a marker for erythroblasts. The number of erythroblasts surrounding each macrophage was significantly reduced in *c-Maf*$^{-/-}$ fetal liver. (B) Erythroblastic islands reconstituted with *c-Maf*$^{+/+}$ erythroblasts were immunostained. The number of *c-Maf*$^{+/+}$ erythroblasts surrounding each *c-Maf*$^{+/+}$ or *c-Maf*$^{-/-}$ macrophage is shown. *c-Maf*$^{+/+}$ erythroblasts surrounding *c-Maf*$^{-/-}$ macrophages were significantly reduced compared with those seen for *c-Maf*$^{+/+}$ macrophages. (C) Erythroblastic islands reconstituted with *c-Maf*$^{-/-}$ erythroblasts were immunostained. The number of *c-Maf*$^{-/-}$ erythroblasts surrounding each *c-Maf*$^{+/+}$ or *c-Maf*$^{-/-}$ macrophage is shown. *c-Maf*$^{-/-}$ erythroblasts surrounding *c-Maf*$^{-/-}$ macrophage were significantly reduced compared with those seen for *c-Maf*$^{+/+}$ macrophages. Although *c-Maf*$^{-/-}$ erythroblasts can form reconstituted erythroblastic islands with *c-Maf*$^{+/+}$ macrophages, *c-Maf*$^{-/-}$ macrophages showed impaired formation of reconstituted erythroblastic islands with *c-Maf*$^{+/+}$ erythroblasts. Images were acquired by a Biorevo BZ microscope (Plan Apo 20×0.75 DIC N2) at room temperature and processed with the Adobe Photoshop CS4 software. The scale bar represents 20 μm; n = 4–6 embryos per group. For each combination, ≥ 20 macrophages per embryo were analyzed. *$P < .05$. Data are presented as mean ± SEM.

number of CFU-E–, BFU-E–, and CFU-GEMM–derived colonies per fetal liver (Figure 3E). In addition, CFU-E colonies were indistinguishable in structure and size (supplemental Figure 4A-B). Moreover, erythroid cells derived from *c-Maf*$^{-/-}$ CFU-Es exhibited a similar structure, and enucleated red blood cells were also similar to those from *c-Maf*$^{+/+}$ control CFU-Es in cytospin slides stained with May-Grünwald-Giemsa (supplemental Figure 4C). Taken together, these results suggest that *c-Maf*$^{-/-}$ erythroid cells are still capable of developing into mature cells in vitro, in contrast to the result of flow cytometric analysis with the use of fetal liver cells (Figures 3A-C; supplemental Figure 2A-B), which reflects the in vivo condition. Therefore, the impaired definitive erythropoiesis in the *c-Maf*$^{-/-}$ embryos is more likely because of a non–cell-autonomous effect of c-Maf deficiency.

Absence of c-Maf causes impaired erythroblastic island formation in the fetal liver

c-Maf is abundantly expressed in fetal liver macrophages, although it is largely missing from the erythroid cells in fetal liver. Therefore, we initially surmised that c-Maf deficiency in fetal liver macrophages disturbed the erythroblastic islands.[3] To address this hypothesis, we attempted to examine whether *c-Maf*$^{-/-}$ macrophages failed to maintain the erythroblastic islands. For this purpose, we isolated the erythroblastic island from *c-Maf*$^{+/+}$ and *c-Maf*$^{-/-}$ fetal livers and counted the number of erythroblasts associated with each single central macrophage according to a previously described method.[31]

Interestingly, although > 10 TER-119^{+} erythroblasts were adhered to a F4/80^{+} macrophage in *c-Maf*$^{+/+}$ fetal livers, c-Maf–deficient central macrophages seemed to harbor far fewer erythroblasts (Figure 4). As shown in Figure 4A, the number of erythroblasts attached to a single central macrophage was significantly reduced in *c-Maf*$^{-/-}$ erythroblastic islands (14.2 ± 0.3 and 5.6 ± 1.5 erythroblasts per macrophage for *c-Maf*$^{+/+}$ and *c-Maf*$^{-/-}$, respectively). This result clearly indicates that erythroblastic islands are impaired in the *c-Maf*$^{-/-}$ fetal livers.

Next, to address whether c-Maf deficiency in macrophages was specifically responsible for the impairment of erythroblastic islands, a series of reconstitution experiments was performed. After attaching native erythroblastic islands either from *c-Maf*$^{+/+}$ or *c-Maf*$^{-/-}$ fetal livers on a glass coverslip, the adherent erythroblasts in the islands were stripped from the macrophages. Next, the

Table 2. Expression of genes comprising the macrophage signature

Symbol	Official full name	*c-Maf*$^{+/+}$ signal	*c-Maf*$^{-/-}$ signal	Fold
VCAM-1	Vascular cell adhesion molecule 1	8.3	1.6	0.19
Mrc1	Mannose receptor, C type 1	19.8	5.7	0.29
Csf1r	Colony stimulating factor 1 receptor	45	16.8	0.37
Sell	Selectin, lymphocyte	26.7	10	0.37
Lamp2	Lysosomal-associated membrane protein 2	8.9	3.3	0.37
Itgav	Integrin α V	1.2	0.5	0.41
Maea (EMP)	Macrophage erythroblast attacher	26.2	14.5	0.55
Emr1 (F4/80)	EGF-like module containing, mucin-like, hormone receptor-like sequence 1	71.4	48.1	0.67
Itgam (Mac-1)	Integrin α M	5.8	3.9	0.67
Cd163	CD163 antigen	0.6	0.4	0.67
Cd14	CD14 antigen	11.8	9.4	0.80
Fcgr1	Fc receptor, IgG, high-affinity I	15.7	17.6	1.12

Fetal liver macrophages were purified by flow cytometry from *c-Maf*$^{+/+}$ or *c-Maf*$^{-/-}$ fetal livers. The fold change in the gene expression was determined by dividing the signal obtained with *c-Maf*$^{-/-}$ fetal liver macrophage RNA by the signal obtained with *c-Maf*$^{+/+}$ RNA.

freshly isolated erythroblasts from *c-Maf*$^{+/+}$ or *c-Maf*$^{-/-}$ fetal livers were cocultured on the remaining adherent *c-Maf*$^{+/+}$ or *c-Maf*$^{-/-}$ fetal liver macrophages, respectively, so that *c-Maf*$^{+/+}$ erythroblasts were cocultured on *c-Maf*$^{-/-}$ central macrophages and vice versa. Surprisingly, *c-Maf*$^{-/-}$ macrophages failed to support erythroblastic islands with the inoculated wild-type

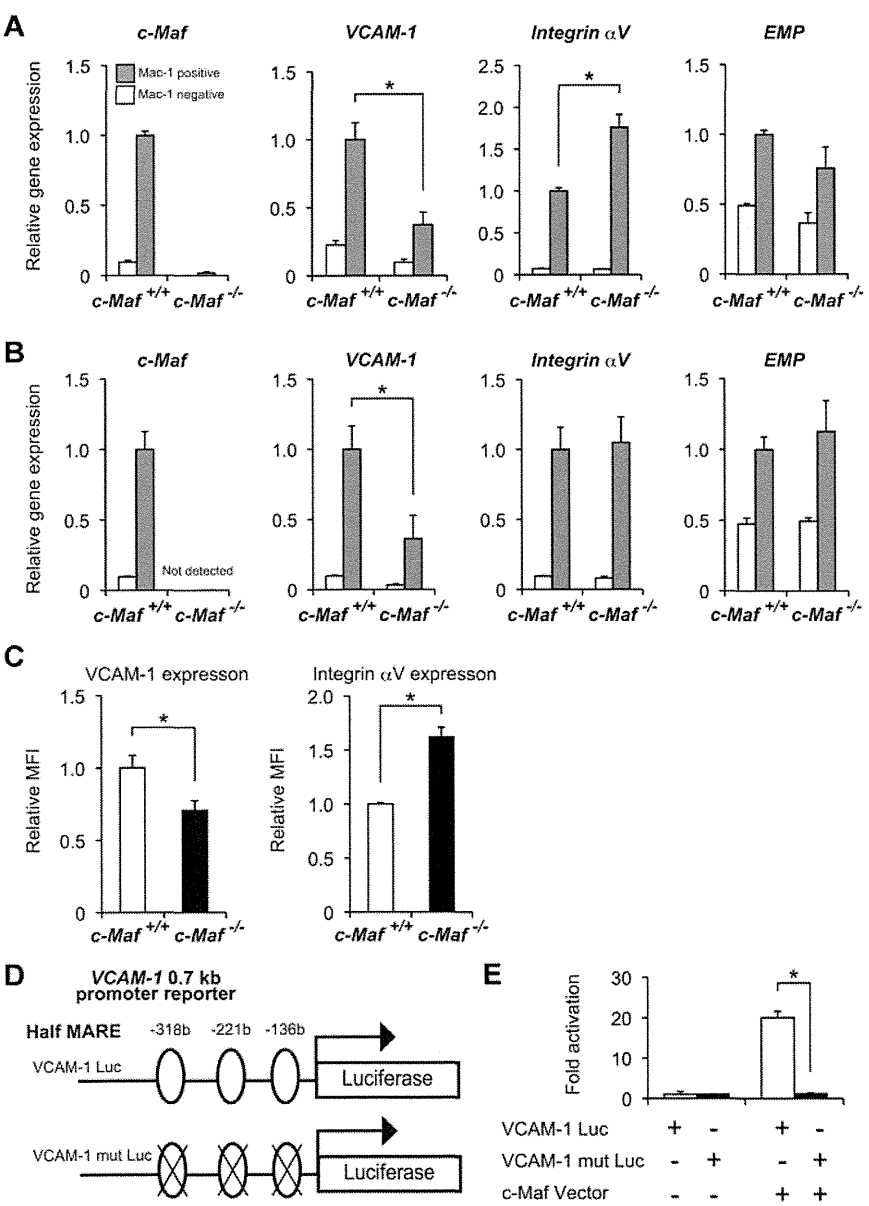

Figure 5. Decreased expression of VCAM-1 in *c-Maf*$^{-/-}$ fetal liver macrophage. mRNA expression profiles of erythroblast-macrophage adhesive interaction genes at E13.5 (A) and at E14.5 (B). Total RNA obtained from the Mac-1$^+$ fraction (gray bar) and Mac-1$^-$ fraction (open bar) of fetal liver cells was used for analyses. VCAM-1 expression was decreased in *c-Maf*$^{-/-}$ macrophages at E13.5 and E14.5; n = 7 per group; $^*P < .05$. The expression level of *c-Maf*$^{+/+}$ fetal liver Mac-1 fraction was set to 1.0. All of the data are presented as mean ± SEM (C) Relative mean fluorescent intensity (MFI) values of VCAM-1 and Integrin αV for the *c-Maf*$^{+/+}$ fetal liver Mac-1 fraction (normalized to MFI = 1) and the *c-Maf*$^{-/-}$ fetal liver Mac-1 fraction. E13.5 fetal liver cells were stained with FITC-conjugated anti–Mac-1 mAb, APC-conjugated anti–VCAM-1 mAb, and PE-conjugated anti-Integrin αV mAb. Bar graphs represent mean ratio ± SEM. Consistent with real-time RT-PCR analysis, significant differences in VCAM-1 and Integrin αV protein expression were observed; n = 8 per group; $^*P < .05$. (D) Schematic diagram of a luciferase reporter construct with the use of a VCAM-1 0.7-kb promoter (VCAM-1 Luc, top) ligated to a firefly luciferase cassette. Three putative half-MARE sites (5′ −318 bp, −221 bp, and −136 bp) are indicated. A luciferase assay was performed with a VCAM-1 Luc and that with mutations in half-MARE (VCAM-1 mut Luc, bottom) as reporters. (E) The pEFX3-FLAG-cMaf expression vector (c-Maf Vector) was cotransfected with the reporter plasmid into the macrophage cell line J774. The relative luciferase activity shown is derived from averages of 2 independent experiments (shown as mean ± SEM). The luciferase activity seen in J774 cells transfected with the reporter plasmid and with an empty vector was normalized to a value of 1 as the standard ($^*P < .05$).

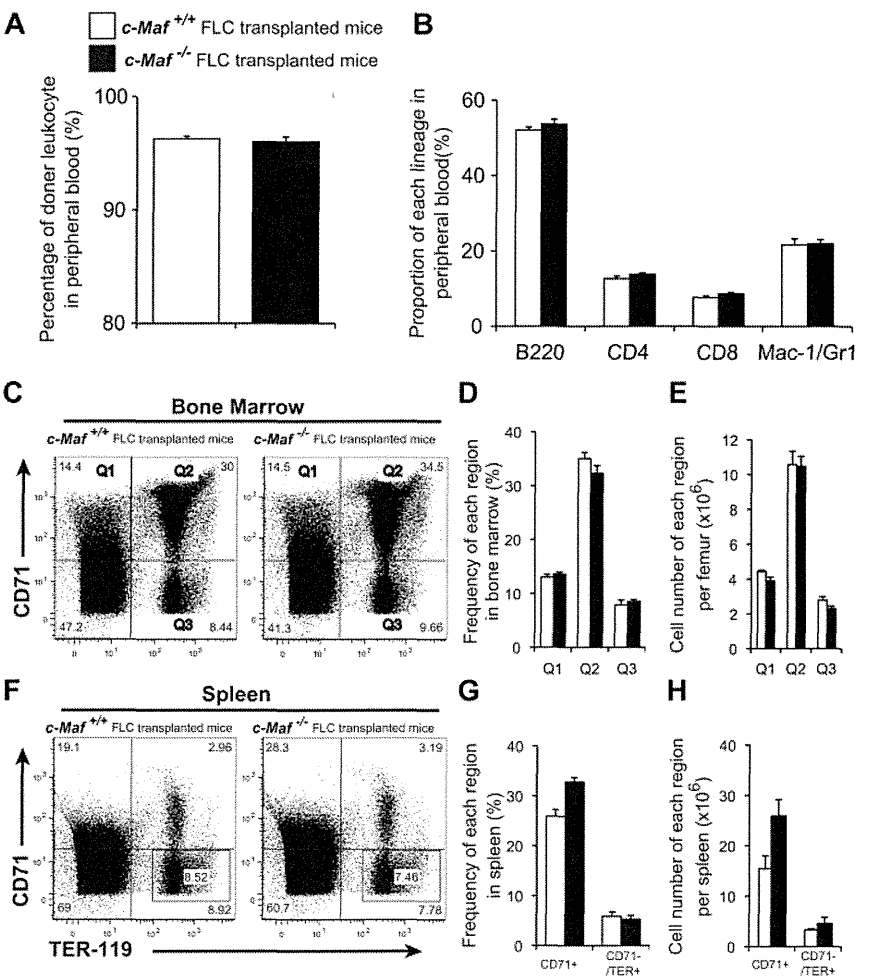

Figure 6. *c-Maf*$^{-/-}$ fetal liver cells can reconstitute adult hematopoiesis in lethally irradiated mice. (A) Eight to 10 weeks after transplantation, the donor leukocyte chimerism of the mice reconstituted with *c-Maf*$^{-/-}$ fetal liver cells was comparable to that of the mice reconstituted with *c-Maf*$^{+/+}$ fetal liver cells. The reconstitution efficiency was checked by flow cytometry with the use of the Ly5.1/Ly5.2 ratio of peripheral blood cells. Donor chimerism was determined to be as follows: (%Ly5.1$^+$/%Ly5.1$^+$ + %Ly5.2$^+$) × 100. (B) No significant difference was found in the proportion of each lineage in peripheral blood between *c-Maf*$^{+/+}$ fetal liver cells transplanted into mice and *c-Maf*$^{-/-}$ fetal liver cells transplanted into mice. (C) Flow cytometric analyses of the TER-119 and CD71 expression in total BM cells prepared from the femur of mice that received a transplant with *c-Maf*$^{+/+}$ fetal liver cells (left) or *c-Maf*$^{-/-}$ fetal liver cells (right). The gates of CD71$^+$/TER-119$^-$ (top left region: Q1), CD71$^+$/TER-119$^+$ (top right region: Q2), and CD71$^-$/TER-119$^+$ (bottom right region: Q3) in BM cells are defined as indicated. (D) Frequencies (%) of cells found in each region are shown. (E) Cell numbers of each region per femur are shown. (F) Flow cytometric analyses of the TER-119 and CD71 expression in total spleen cells prepared from mice that received a transplant with *c-Maf*$^{+/+}$ fetal liver cells (left) and *c-Maf*$^{-/-}$ fetal liver cells (right). The frequencies (%) of CD71$^+$ (top left and top right regions) and CD71$^-$/TER-119$^+$ (indicated squared gate in the bottom right region) cells in the spleen are indicated. (G) Frequencies (%) of each region are shown. (H) Cell numbers of each region per spleen are shown. Note that there are no significantly different frequencies or numbers of BM or spleen cells between mice that received a transplant with *c-Maf*$^{+/+}$ fetal liver cells versus with *c-Maf*$^{-/-}$ fetal liver cells. □ represents mice that received a transplant with *c-Maf*$^{+/+}$ fetal liver cells; ■, mice that received a transplant with *c-Maf*$^{-/-}$ fetal liver cells; n = 4 per group. FLC indicates, fetal liver cell.

erythroblasts (12.7 ± 0.5 erythroblasts per *c-Maf*$^{+/+}$ macrophage and 4.8 ± 0.2 erythroblasts per *c-Maf*$^{-/-}$ macrophage; Figure 4B). In contrast, *c-Maf*$^{-/-}$ erythroblasts were still capable of attaching to *c-Maf*$^{+/+}$ macrophages to the same extent as wild-type erythroblasts (13.9 ± 0.5 erythroblasts per *c-Maf*$^{+/+}$ macrophage and 5.1 ± 0.4 erythroblasts per *c-Maf*$^{-/-}$ macrophage; Figure 4C). These results show that the erythropoietic defects in *c-Maf*$^{-/-}$ embryos could be induced by an impaired hematopoietic microenvironment. Most probably, the suppressed functions of c-Maf–deficient central macrophages were responsible for the damaged erythroblastic islands.

Identification of target genes of c-Maf in fetal liver macrophages

To identify the molecular targets by which c-Maf regulates formation of erythroblastic islands in macrophages, we monitored the expression of cell adhesion molecules by microarray analysis. The expression of several important adhesion molecules was decreased in *c-Maf*$^{-/-}$ macrophages (Table 2). Expression of *VCAM-1* was suppressed the furthest in these molecules. To confirm the results from microarray analysis, we performed quantitative RT-PCR analyses, examining expression levels of *VCAM-1*, *Integrin* α*V*, and *EMP*. These are essential for erythroblastic island formation and maintenance and are thus designated as erythroblast-macrophage adhesive molecules.[3] The Mac-1$^+$ cells from either E13.5 or E14.5 fetal liver were sorted and analyzed to determine the mRNA abundance of these genes by real-time RT-PCR analysis. Of note, we observed an ~ 2.5-fold reduction in the *VCAM-1* mRNA expression level in the Mac-1$^+$ fraction from *c-Maf*$^{-/-}$ fetal liver, compared with the *c-Maf*$^{+/+}$ control at E13.5 and E14.5 (Figure 5A-B). However, *EMP* mRNA expression was not reduced in *c-Maf*$^{-/-}$ compared with *c-Maf*$^{+/+}$ (Figure 5A-B). In addition, expression of *Integrin* α*V* at E13.5 in *c-Maf*$^{-/-}$ was significantly up-regulated. Consistent with this observation, flow cytometric analysis of the fetal liver cells at E13.5 also verified a significant reduction of VCAM-1 protein expression in the *c-Maf*$^{-/-}$ fetal liver Mac-1$^+$ cells compared with the *c-Maf*$^{+/+}$ fetal liver Mac-1$^+$ cells, and protein expression of Integrin αV in the *c-Maf*$^{-/-}$ fetal liver Mac-1$^+$ cells was higher than that in *c-Maf*$^{+/+}$ (Figure 5C).

Given the significant suppression of VCAM-1 expression in *c-Maf*$^{-/-}$ fetal liver macrophages, we next addressed whether c-Maf could activate the *VCAM-1* gene promoter. To this end, a luciferase reporter assay in the J774 macrophage cell line was performed with a plasmid containing the 0.7-kb *VCAM-1* promoter region (VCAM-1 Luc) as a reporter (Figure 5D). The luciferase activity was significantly increased when the reporter plasmid was cotransfected with an expression plasmid for c-Maf. In contrast, when putative half-MARE sequences were mutated (VCAM-1 mut Luc), activation of the reporter was blunted (Figure 5E). These results indicate that c-Maf regulates the expression of *VCAM-1* by binding the putative half-MARE sites in its promoter region.

Table 3. Blood cell counts 6-12 weeks after fetal liver cell transplantation in mice

Genotype of transplanted FLC	*c-Maf*$^{+/+}$	*c-Maf*$^{-/-}$
WBC count, /μL	14 100 ± 1500	13 500 ± 1400
RBC count, ×10^4/μL	967 ± 10.0	949 ± 11.0
Hb level, g/dL	14.1 ± 0.2	13.9 ± 0.2
HCT, %	47.1 ± 0.7	46.8 ± 0.7
MCV, fL	48.7 ± 0.5	49.3 ± 0.4
MCH, pg	14.6 ± 0.2	14.6 ± 0.1
PLT count, ×10^4/μL	102.6 ± 5.8	92.3 ± 4.6

Values shown are the mean ± SEM for 20 mice per genotype. Mice with ≥ 90% donor leukocyte chimerism were used for analysis. *P* values were all NS.

FLC indicates fetal liver cell; WBC, white blood cell; RBC, red blood cell; Hb, hemoglobin; HCT, hematocrit; MCV, mean corpuscular volume; MCH, mean corpuscular hemoglobin; and PLT, platelet.

c-Maf–deficient fetal liver cells are capable of reconstituting the hematopoietic system of adult mice

To determine whether *c-Maf*$^{-/-}$ embryos still retain functional hematopoietic stem cells, we tested the ability of *c-Maf*–deficient fetal liver cells to reconstitute the hematopoietic system of lethally irradiated recipient mice. Fetal liver cells collected from E14.5 *c-Maf*$^{+/+}$ or *c-Maf*$^{-/-}$ embryos were injected into lethally irradiated recipient mice. All recipients receiving both *c-Maf*$^{+/+}$ and *c-Maf*$^{-/-}$ fetal liver cells survived and remained healthy for ≥ 6 months after transplantation. The donor-derived leukocyte chimerism in the mice reconstituted with *c-Maf*$^{-/-}$ fetal liver cells was comparable with that of the recipient mice with control fetal liver cells (Figure 6A). Moreover, there were no significant differences in hematocrit or proportion (%) of B220$^+$, CD4$^+$, CD8$^+$, or Mac-1$^+$/Gr1$^+$ cells between the recipients receiving *c-Maf*$^{+/+}$ or *c-Maf*$^{-/-}$ fetal liver cells (Table 3; Figure 6B).

Next, we attempted to examine whether erythroblast differentiation in the BM and spleen was perturbed. The absolute number of BM cells (19.9 ± 1.69 and 18.3 ± 1.56 × 10^6 cells/femur for *c-Maf*$^{+/+}$ and *c-Maf*$^{-/-}$ fetal liver cells transplanted into mice, respectively) as well as the spleen weight (68.4 ± 3.28 and 73.8 ± 5.44 mg for *c-Maf*$^{+/+}$ and *c-Maf*$^{-/-}$ fetal liver cells transplanted into mice, respectively) were comparable between mice that received a transplant with *c-Maf*$^{+/+}$ and *c-Maf*$^{-/-}$ fetal liver cells. Each stage of the erythroblasts was prospectively separated by a flow cytometric protocol that used TER-119 and CD71 Abs. The frequencies and cell numbers of each region in the recipient BM receiving *c-Maf*$^{-/-}$ fetal liver cells were comparable to those in the recipient with *c-Maf*$^{+/+}$ fetal liver cells (Figure 6C-E). Similar results were also observed with spleen cells (Figure 6F-H). Applying another method that TER-119 and CD44 Abs,[30] we assessed erythropoiesis in the BM of the mice that received a transplant. The differentiation status was found to be comparable between the recipients with *c-Maf*$^{+/+}$ and *c-Maf*$^{-/-}$ fetal liver cells (supplemental Figure 5A-C). Overall, these results indicate that *c-Maf*$^{-/-}$ hematopoietic cells are able to reconstitute the hematopoietic system in lethally irradiated mice and that they have the ability to produce adequate amounts of erythroid cells.

c-Maf deficiency does not impair erythropoiesis during PHZ-induced anemia

To assess the role of c-Maf in adult hematopoiesis further, we analyzed BM macrophages in a similar manner as that used to analyze fetal liver cells. The donor-derived BM leukocyte and BM macrophage chimerisms in the mice reconstituted with *c-Maf*$^{-/-}$ fetal liver cells were comparable with those of the recipient mice with control fetal liver cells (supplemental Figure 6). To determine whether *VCAM-1* mRNA levels were decreased, Mac-1$^+$ cells from the BM of mice that received a transplant were sorted and analyzed for mRNA abundance of *Mac-1*, *c-Maf*, *VCAM-1*, and *Integrin* α*V* by real-time RT-PCR analysis. These experiments showed no differences in expression levels in mice that received a transplant with *c-Maf*$^{+/+}$ and *c-Maf*$^{-/-}$ fetal liver cells except for *c-Maf* (Figure 7A), in contrast to the results obtained with the use of fetal

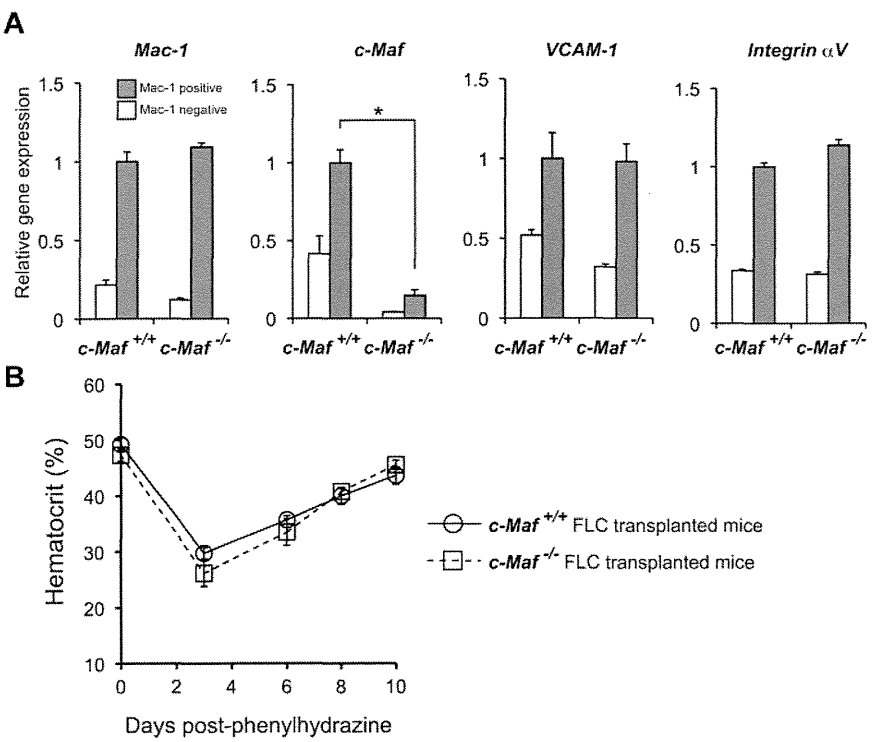

Figure 7. Responses of mice that received a transplant with *c-Maf*$^{-/-}$ fetal liver cells to induce anemia. (A) Comparisons of mRNA expression of *Mac-1*, *c-Maf*, *VCAM-1*, and *Integrin* α*V* are shown. Total RNA obtained from the Mac-1$^+$ positive fraction (gray bar) and the Mac-1$^-$ fraction (open bar) of BM cells was used for analyses. Note that *VCAM-1* mRNA expression of the Mac-1$^+$ fraction in mice that received a transplant with *c-Maf*$^{-/-}$ fetal liver cells is comparable with that of control mice that received a transplant with *c-Maf*$^{+/+}$ fetal liver cells; n = 5 per group; FLC indicates fetal liver cell; Expression of the *c-Maf*$^{+/+}$ BM Mac-1 fraction was set to 1.0. All of the data are presented as mean ± SEM. (B) Mice with a baseline hematocrit of ≥ 35% were used. Four mice that received a transplant with *c-Maf*$^{+/+}$ fetal liver cells (open circle with solid line) and 4 mice that received a transplant with *c-Maf*$^{-/-}$ fetal liver cells (open square with dashed line) were injected with phenylhydrazine on days 0, 1, and 3. Hematocrit levels were assessed on days 0, 3, 6, 8, and 10. Data are mean ± SEM.

liver cells. To reconfirm these results with a functional assay, mice were challenged with PHZ, and their hematocrits were monitored for the next 10 days (Figure 7B). The hematocrits of mice from both groups were comparable during this period. These results indicate that c-Maf deficiency does not impair stress erythropoiesis during PHZ-induced anemia in adult mice.

Discussion

Macrophages are important for hematopoiesis because they engulf nuclei of erythroblasts in erythroblastic islands, where the macrophages are surrounded by erythroblasts in the fetal liver, BM, and spleen.[3] In the present study, we demonstrated that c-Maf is crucial for the function of macrophages in erythropoiesis.

Our study clearly shows that disruption of c-Maf causes impaired erythroblastic island formation because of dysfunction of fetal liver macrophages. In a methylcellulose culture system, *c-Maf*$^{-/-}$ hematopoietic stem/progenitor cells in fetal liver have a normal potential to differentiate into different lineages, and they can reconstitute the hematopoietic system of lethally irradiated mice. Because c-Maf is specifically expressed in macrophages within the fetal liver, it has been thought that c-Maf does not regulate fetal liver erythropoiesis through a function of erythroblasts, but rather that it performs an adhesive function of macrophages. There are several reports of genes that are related to the formation and maintenance of erythroblastic islands, based on the knockout mice technique. Retinoblastoma-deficient mice were analyzed for macrophage differentiation, and erythroblastic island formation was reported to be impaired in these mice.[31] The fetal livers of *Dnase2a*$^{-/-}$ mice contain many macrophages that carry undigested DNA, and IFN-β mRNA was expressed by the resident macrophages in the *Dnase2a*$^{-/-}$ fetal liver.[37,38] In *c-Maf*$^{-/-}$ fetal livers, retinoblastoma was comparably expressed in *c-Maf*$^{+/+}$ and *c-Maf*$^{-/-}$ macrophages; therefore, the existence of impaired erythroblastic islands in *c-Maf*$^{-/-}$ mice is not related to retinoblastoma (supplemental Figure 7). In addition, we could not detect the abnormal foci that are found in *Dnase2a*$^{-/-}$ fetal livers or the expression of *IFN*-β mRNA (data not shown). Thus, retinoblastoma or DNase II do not cause the impaired erythroblastic islands of *c-Maf*$^{-/-}$ embryos.

To identify the target genes of c-Maf in fetal liver macrophages, we performed microarray analysis and found that VCAM-1 was one of these target genes. VCAM-1 is an adhesion molecule expressed on macrophages of erythroblastic islands. Previous studies have shown that maintenance of erythroblastic islands was impaired by an anti–VCAM-1 Ab.[8,39] As shown in Figure 5, mRNA and cell surface protein expression of VCAM-1 was decreased in *c-Maf*$^{-/-}$ fetal liver macrophages. This suggests that decreased expression of *VCAM-1* may be at least in part responsible for impaired erythroblastic island maintenance in *c-Maf*$^{-/-}$ fetal liver. The large Maf proteins are known to bind MAREs or the 5′ AT-rich half-MARE. In the *VCAM-1* promoter region, there are 3 half-MARE sites, so c-Maf may directly regulate *VCAM-1* expression in fetal liver macrophages. Recently, Kohyama et al[40] revealed that Spi-C controls the development of red pulp macrophages required for red blood cell recycling, and it regulates *VCAM-1* expression in red pulp macrophages. These earlier results and ours suggest that the regulation of *VCAM-1* expression by transcription factors strongly affects the function of tissue macrophages. In macrophages, c-Maf regulates the expression of cell surface molecules that are involved in macrophage function. In this analysis, expression of Integrin αV in *c-Maf*$^{-/-}$ macrophages was transiently up-regulated. It is difficult to identify the mechanism, but it seems probable there may be a compensation mechanism causing down-regulation of VCAM-1 in fetal macrophages.

We found that c-Maf is crucial for erythroblastic island maintenance in the embryonic stage. In a reconstitution assay that used fetal liver cells, *c-Maf*$^{-/-}$ hematopoietic cells reconstituted hematopoiesis in lethally irradiated mice, and the mice that received a transplant with *c-Maf*$^{-/-}$ fetal liver cells did not show anemia in the steady state (Table 3). To test the function of c-Maf in the adult stage further, we analyzed the mice that received a transplant by BM cell assay and by a PHZ stress test. Neither decreased expression level of *VCAM-1* mRNA nor impaired erythroid differentiation were observed. In addition, the response to the PHZ stress test was also comparable between the 2 groups. These results indicate that c-Maf might activate the VCAM-1 gene and affect erythroblastic island maintenance in a context-dependent manner. Such observations were reported previously. In *Palld*$^{-/-}$ fetal liver, erythroblastic island formation or integrity was impaired, but *Palld*$^{-/-}$ fetal liver cells could reconstitute the blood of lethally irradiated mice.[6] Thus, c-Maf and Palladin are important for erythroblastic islands in the embryonic stage, but their importance in the adult stage is still unconfirmed. However, a previous study found that ICAM-4 is critical for erythroblastic island formation in adult marrow,[41] but the role of ICAM-4 in the embryonic stage has been left for future study. Overall, previous studies and our results indicate that there might be different mechanisms or regulation processes or both between fetal liver and adult marrow/spleen erythroblastic island formation and maintenance. This suggests that macrophages in fetal liver and in the adult marrow/spleen might have different developmental origins. Further studies are needed to investigate this possibility.

Recent reports have indicated that definitive as well as primitive erythropoiesis are related to erythroblastic islands.[39] Kingsley et al[42] revealed that yolk sac-derived primitive erythroblasts enucleate during gestation, and Isern et al[39] and Fraser et al[43] also have demonstrated, using transgenic mouse lines, that primitive erythroblasts enucleate within the fetal liver.[39,43] Our quantitative RT-PCR results suggested that definitive erythropoiesis is more involved in erythroblastic islands than is primitive erythropoiesis in vivo (supplemental Figure 3). Therefore, this result indicates that definitive erythropoiesis in fetal liver is predominantly impaired in *c-Maf*$^{-/-}$ embryos, whereas primitive erythropoiesis is maintained in *c-Maf*$^{-/-}$ embryos.

Our study showed that *c-Maf*$^{-/-}$ mice were embryonic lethal on the C57BL/6 background and that *c-Maf*$^{-/-}$ macrophages might be responsible for this. Previous reports from our laboratory and from others indicated that *c-Maf*$^{-/-}$ mice were lethal around birth on the C57BL/6J × 129/SV background, but some mice on the BALB/c background live to adulthood.[14,44,45] It is known that cytokine production in T-helper cells differs between C57BL/6 and BALB/c backgrounds. Recently Mills at al[46] reported that cytokine production in macrophages differed according to the backgrounds of the mice. On a C57BL/6 background, inflammatory cytokine production is more dominant than on a BALB/c background. It is well known that apoptotic cells are recognized by macrophages and induce the production of proinflammatory cytokines.[47] Increased amounts of apoptotic cells were observed in *c-Maf*$^{-/-}$ fetal liver, suggesting that inflammatory cytokine production might be triggered in *c-Maf*$^{-/-}$ fetal liver. Therefore, our *c-Maf*$^{-/-}$ mice were lethal at an earlier gestational date than indicated by previous reports. We found that *c-Maf*$^{-/-}$ fetal liver macrophages produced

more cytokines than *c-Maf*$^{+/+}$ fetal liver macrophages (supplemental Figure 7). Hence, it is tempting to speculate that increased numbers of apoptotic cells trigger the production of inflammatory cytokines that are reported to be responsible for anemia and embryonic lethality. This speculation supports the idea that the *c-Maf*$^{-/-}$ macrophages are responsible for anemia and lethality. This hypothesis may also explain the phenotype discrepancy between *c-Maf*$^{-/-}$ mice and *F4/80*$^{-/-}$ or *VCAM-1*$^{-/-}$ mice. Neither F4/80 knockout mice nor mice with a conditional ablation of VCAM-1 in blood cells are embryonic lethal.[48-50] In addition, c-Maf is a transcription factor, and it might regulate sets of target genes in fetal macrophages that might in turn be responsible for the observed anemia and lethality.

In summary, we have shown that the transcription factor c-Maf gene affects the hematopoietic microenvironment by playing a crucial role in regulating fetal liver macrophages.

Acknowledgments

The authors thank Dr Yamashita and Dr Ohneda for the *VCAM-1* promoter containing luciferase plasmid.

This work was supported by a Grant-in-Aid for Scientific Research (KAKENHI no. 21220009) from the Ministry of Education, Culture, Sports, Science and Technology of Japan (MEXT). This work was also supported by Grants from the Astellas Foundation for Research on Metabolic Disorders and the Uehara Memorial Foundation. M.K. is a recipient of a Japan Society for the Promotion of Science Research Fellowship for Young Scientists (21384).

Authorship

Contribution: M.K., K.H., M.H., M.N., T.O., H.S., and M.T.N.T. performed experiments; M.K., K.H., and M.H. analyzed results and made figures; M.K., K.H., M.H., and S.T. designed the research; M.K., M.H., and S.T. wrote the paper; K.U. performed microarray analysis; and T.K., H.N., S.C., and S.T. supervised the project.

Conflict-of-interest disclosure: The authors declare no competing financial interests.

Correspondence: Satoru Takahashi, Departments of Anatomy and Embryology, Institute of Basic Medical Science, University of Tsukuba, 1-1-1 Tennodai, Tsukuba, Ibaraki 305-8575, Japan; e-mail: satoruta@md.tsukuba.ac.jp.

References

1. Palis J. Ontogeny of erythropoiesis. *Curr Opin Hematol.* 2008;15(3):155-161.
2. Allen TD, Dexter TM. Ultrastructural aspects of erythropoietic differentiation in long-term bone marrow culture. *Differentiation.* 1982;21(2):86-94.
3. Chasis JA, Mohandas N. Erythroblastic islands: niches for erythropoiesis. *Blood.* 2008;112(3): 470-478.
4. Hanspal M, Hanspal JS. The association of erythroblasts with macrophages promotes erythroid proliferation and maturation: a 30-kD heparin-binding protein is involved in this contact. *Blood.* 1994;84(10):3494-3504.
5. Mohandas N, Prenant M. Three-dimensional model of bone marrow. *Blood.* 1978;51(4):633-643.
6. Liu X-S, Li X-H, Wang Y, et al. Disruption of palladin leads to defects in definitive erythropoiesis by interfering with erythroblastic island formation in mouse fetal liver. *Blood.* 2007;110(3):870-876.
7. Soni S, Bala S, Gwynn B, Sahr KE, Peters LL, Hanspal M. Absence of erythroblast macrophage protein (Emp) leads to failure of erythroblast nuclear extrusion. *J Biol Chem.* 2006;281(29): 20181-20189.
8. Sadahira Y, Yoshino T, Monobe Y. Very late activation antigen 4-vascular cell adhesion molecule 1 interaction is involved in the formation of erythroblastic islands. *J Exp Med.* 1995;181(1):411-415.
9. Nishizawa M, Kataoka K, Goto N, Fujiwara KT, Kawai S. v-maf, a viral oncogene that encodes a "leucine zipper" motif. *Proc Natl Acad Sci U S A.* 1989;86(20):7711-7715.
10. Kataoka K, Fujiwara KT, Noda M, Nishizawa M. MafB, a new Maf family transcription activator that can associate with Maf and Fos but not with Jun. *Mol Cell Biol.* 1994;14(11):7581-7591.
11. Kataoka K, Noda M, Nishizawa M. Maf nuclear oncoprotein recognizes sequences related to an AP-1 site and forms heterodimers with both Fos and Jun. *Mol Cell Biol.* 1994;14(1):700-712.
12. Yoshida T, Ohkumo T, Ishibashi S, Yasuda K. The 5′-AT-rich half-site of Maf recognition element: a functional target for bZIP transcription factor Maf. *Nucleic Acids Res.* 2005;33(11): 3465-3478.
13. Kajihara M, Kawauchi S, Kobayashi M, Ogino H, Takahashi S, Yasuda K. Isolation, characterization, and expression analysis of zebrafish large Mafs. *J Biochem.* 2001;129(1):139-146.
14. Kawauchi S, Takahashi S, Nakajima O, et al. Regulation of lens fiber cell differentiation by transcription factor c-Maf. *J Biol Chem.* 1999;274(27): 19254-19260.
15. Moriguchi T, Hamada M, Morito N, et al. MafB is essential for renal development and F4/80 expression in macrophages. *Mol Cell Biol.* 2006; 26(15):5715-5727.
16. Ogino H, Yasuda K. Induction of lens differentiation by activation of a bZIP transcription factor, L-Maf. *Science.* 1998;280(5360):115-118.
17. Sieweke MH, Tekotte H, Frampton J, Graf T. MafB is an interaction partner and repressor of Ets-1 that inhibits erythroid differentiation. *Cell.* 1996;85(1):49-60.
18. Swaroop A, Xu JZ, Pawar H, Jackson A, Skolnick C, Agarwal N. A conserved retina-specific gene encodes a basic motif/leucine zipper domain. *Proc Natl Acad Sci U S A.* 1992;89(1):266-270.
19. Zhang C, Moriguchi T, Kajihara M, et al. MafA is a key regulator of glucose-stimulated insulin secretion. *Mol Cell Biol.* 2005;25(12):4969-4976.
20. Eychene A, Rocques N, Pouponnot C. A new MAFia in cancer. *Nat Rev Cancer.* 2008;8(9):683-693.
21. Hurt EM, Wiestner A, Rosenwald A, et al. Overexpression of c-maf is a frequent oncogenic event in multiple myeloma that promotes proliferation and pathological interactions with bone marrow stroma. *Cancer Cell.* 2004;5(2):191-199.
22. Morito N, Yoh K, Fujioka Y, et al. Overexpression of c-Maf contributes to T-cell lymphoma in both mice and human. *Cancer Res.* 2006;66(2):812-819.
23. Murakami YI, Yatabe Y, Sakaguchi T, et al. c-Maf expression in angioimmunoblastic T-cell lymphoma. *Am J Surg Pathol.* 2007;31(11):1695-1702.
24. Bauquet AT, Jin H, Paterson AM, et al. The costimulatory molecule ICOS regulates the expression of c-Maf and IL-21 in the development of follicular T helper cells and TH-17 cells. *Nat Immunol.* 2009;10(2):167-175.
25. Ho IC, Hodge MR, Rooney JW, Glimcher LH. The proto-oncogene c-maf is responsible for tissue-specific expression of interleukin-4. *Cell.* 1996; 85(7):973-983.
26. Cao S, Liu J, Song L, Ma X. The protooncogene c-Maf is an essential transcription factor for IL-10 gene expression in macrophages. *J Immunol.* 2005;174(6):3484-3492.
27. Aziz A, Soucie E, Sarrazin S, Sieweke MH. MafB/c-Maf deficiency enables self-renewal of differentiated functional macrophages. *Science.* 2009; 326(5954):867-871.
28. Nakamura M, Hamada M, Hasegawa K, et al. c-Maf is essential for the F4/80 expression in macrophages in vivo. *Gene.* 2009;445(1-2):66-72.
29. Masuoka HC, Townes TM. Targeted disruption of the activating transcription factor 4 gene results in severe fetal anemia in mice. *Blood.* 2002;99(3): 736-745.
30. Chen K, Liu J, Heck S, Chasis JA, An X, Mohandas N. Resolving the distinct stages in erythroid differentiation based on dynamic changes in membrane protein expression during erythropoiesis. *Proc Natl Acad Sci U S A.* 2009;106(41): 17413-17418.
31. Iavarone A, King ER, Dai X-M, Leone G, Stanley ER, Lasorella A. Retinoblastoma promotes definitive erythropoiesis by repressing Id2 in fetal liver macrophages. *Nature.* 2004;432(7020):1040-1045.
32. Ema M, Mori D, Niwa H, et al. Kruppel-like factor 5 is essential for blastocyst development and the normal self-renewal of mouse ESCs. *Cell Stem Cell.* 2008;3(5):555-567.
33. Yamashita T, Ohneda O, Sakiyama A, Iwata F, Ohneda K, Fujii-Kuriyama Y. The microenvironment for erythropoiesis is regulated by HIF-2alpha through VCAM-1 in endothelial cells. *Blood.* 2008;112(4):1482-1492.
34. Angelillo-Scherrer A, Burnier L, Lambrechts D, et al. Role of Gas6 in erythropoiesis and anemia in mice. *J Clin Invest.* 2008;118(2):583-596.
35. Wu L, de Bruin A, Saavedra HI, et al. Extra-embryonic function of Rb is essential for embryonic development and viability. *Nature.* 2003; 421(6926):942-947.
36. Zhang J, Socolovsky M, Gross AW, Lodish HF.

Role of Ras signaling in erythroid differentiation of mouse fetal liver cells: functional analysis by a flow cytometry-based novel culture system. *Blood.* 2003;102(12):3938-3946.

37. Kawane K, Fukuyama H, Kondoh G, et al. Requirement of DNase II for definitive erythropoiesis in the mouse fetal liver. *Science.* 2001;292(5521): 1546-1549.
38. Yoshida H, Okabe Y, Kawane K, Fukuyama H, Nagata S. Lethal anemia caused by interferon-beta produced in mouse embryos carrying undigested DNA. *Nat Immunol.* 2005;6(1):49-56.
39. Isern J, Fraser ST, He Z, Baron MH. The fetal liver is a niche for maturation of primitive erythroid cells. *Proc Natl Acad Sci U S A.* 2008;105(18): 6662-6667.
40. Kohyama M, Ise W, Edelson BT, et al. Role for Spi-C in the development of red pulp macrophages and splenic iron homeostasis. *Nature.* 2009;457(7227):318-321.
41. Lee G, Lo A, Short SA, et al. Targeted gene deletion demonstrates that the cell adhesion molecule ICAM-4 is critical for erythroblastic island formation. *Blood.* 2006;108(6):2064-2071.
42. Kingsley PD, Malik J, Fantauzzo KA, Palis J. Yolk sac-derived primitive erythroblasts enucleate during mammalian embryogenesis. *Blood.* 2004; 104(1):19-25.
43. Fraser ST, Isern J, Baron MH. Maturation and enucleation of primitive erythroblasts during mouse embryogenesis is accompanied by changes in cell-surface antigen expression. *Blood.* 2007;109(1):343-352.
44. Kim JI, Li T, Ho IC, Grusby MJ, Glimcher LH. Requirement for the c-Maf transcription factor in crystallin gene regulation and lens development. *Proc Natl Acad Sci U S A.* 1999;96(7):3781-3785.
45. Ring BZ, Cordes SP, Overbeek PA, Barsh GS. Regulation of mouse lens fiber cell development and differentiation by the Maf gene. *Development.* 2000;127(2):307-317.
46. Mills CD, Kincaid K, Alt JM, Heilman MJ, Hill AM. M-1/M-2 macrophages and the Th1/Th2 paradigm. *J Immunol.* 2000;164(12):6166-6173.
47. Nagata S, Hanayama R, Kawane K. Autoimmunity and the clearance of dead cells. *Cell.* 2010; 140(5):619-630.
48. Lin HH, Faunce DE, Stacey M, et al. The macrophage F4/80 receptor is required for the induction of antigen-specific efferent regulatory T cells in peripheral tolerance. *J Exp Med.* 2005;201(10): 1615-1625.
49. Schaller E, Macfarlane AJ, Rupec RA, Gordon S, McKnight AJ, Pfeffer K. Inactivation of the F4/80 glycoprotein in the mouse germ line. *Mol Cell Biol.* 2002;22(22):8035-8043.
50. Ulyanova T, Scott LM, Priestley GV, et al. VCAM-1 expression in adult hematopoietic and nonhematopoietic cells is controlled by tissue-inductive signals and reflects their developmental origin. *Blood.* 2005;106(1):86-94.

Int J Hematol
DOI 10.1007/s12185-012-1182-y

Splicing factor mutations in myelodysplasia

Seishi Ogawa

Received: 6 September 2012 / Revised: 14 September 2012 / Accepted: 14 September 2012

Abstract Myelodysplastic syndromes (MDS) and related myeloid neoplasms are a heterogeneous group of myeloid neoplasms, which frequently terminate in acute myeloid leukemia (AML). During the past decade, a number of gene mutations have been identified in MDS. However, the spectrum of these mutations overlaps largely with that in AML, complicating the understanding of MDS-specific pathogenesis that discriminates MDS from AML. Recently, several groups reported frequent mutations of multiple components of the RNA splicing machinery in MDS and related disorders. Largely specific to myelodysplastic phenotypes, these splicing factor mutations provide a potential clue to better understanding of the pathogenesis of MDS.

Keywords SF3B1 · U2AF35 · SRSF2 · ZRSR2 · RNA splicing · MDS

Introduction

Myelodysplastic syndromes (MDS) and related myeloid neoplasms are a heterogeneous group of intractable myeloid malignancies, characterized by deregulated blood cell production with dysplastic cell morphology and a high propensity to acute myeloid leukemia (AML) [1]. Over the past 10 years, significant advances have been made in our understanding of the molecular pathogenesis of MDS and other myelodysplasias, including chronic myelomonocytic leukemia (CMML) and atypical chronic myeloid leukemia, through identification of common gene mutations found in these neoplasms [2]. The spectrum of gene mutations in MDS and related myeloid neoplasms includes mutations involving classical signaling molecules, such as *NRAS/KRAS, PTNP11, NF1, c-CBL, JAK2*, and *FLT3*, and those involving hematopoietic transcription factors, such as *RUNX1, ETV6*, and *CEBPA*, together with *TP53* and other tumor suppressor genes. In addition, the recent discovery of frequent mutations of epigenetic regulators engaged in DNA methylation (*DNMT3A, TET2*, and *IDH1/2*) and histone modifications (*ASXL1* and *EZH2* and other components of Polycomb complex 2) in MDS suggested a central role of a compromised epigenetic regulation in their pathogenesis [3]. However, many of these mutations in MDS are observed to some extent in other myeloid neoplasms, including AML and other myelproliferative neoplasms (MPNs), indicating the presence of common mechanisms among different myeloid neoplasms [4]. For example, *DNMT3A, TET2, IDH1/2* and *ASXL1* are among most frequent targets of gene mutations in both MDS and normal karyotype AML [5–10]. A few gene mutations are highly specific to MDS or myelodysplasia, whereas a number of chimeric genes and other mutations, including those in *MPN1* and *CEBPA*, are highly specific to AML [11].

Discovery of frequent mutations of splicing machinery in myelodysplasia

Recently, several groups have reported whole exome sequencing of MDS and other myelodysplasias, in which a common finding was frequent mutations of genes involved in RNA splicing in MDS and related myeloid neoplasms

S. Ogawa (✉)
Cancer Genomics Project, Graduate School of Medicine,
The University of Tokyo, 7-3-1 Hongo,
Bunkyo-ku, Tokyo 113-8655, Japan
e-mail: sogawa-tky@umin.ac.jp

Published online: 05 October 2012

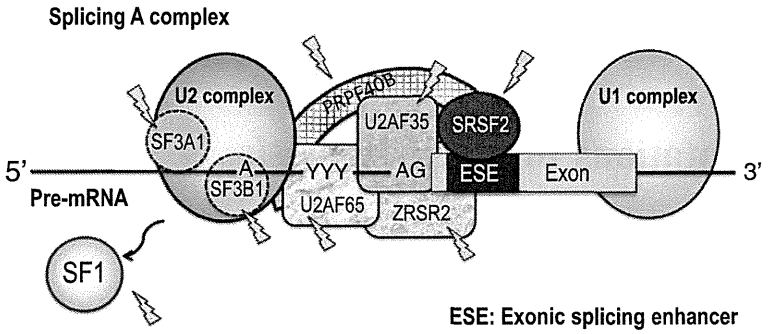

Fig. 1 After the recognition of the 5′ splice site by U1 snRNP complex, a protein complex consisting of a U2AF heterodimer, ZRSR2 and SRSF1/2 was recruited to the 3′ splice boundary, where the smaller subunit (U2AF35) of the U2AF heterodimer binds to the AG-dinucleotide, while the larger subunits recognize a polypyrimidine tract. SRSF1 and SRSF2 belong to a SR family of proteins, having one or more Serine–Arginine-rich domains, and bind to splicing enhancer sequences and also interact with other proteins through its SR domain. To the 5′ upstream of the polypyrimidine tract lies a branchpoint sequence, to which another splicing factor, SF-1, binds and together with the U2AF heterodimer and other components, participates in the establishment of the splicing E complex. Once the splicing E complex is established, a U2 snRNP complex replaces SF-1 to generate the splicing A complex. Prominently, all the major components of these splicing complex are targets of gene mutations in MDS

[12–15]. Through the whole exome sequencing of nine cases with low risk MDS, of which eight were MDS with ring sideroblasts, Papaemmanuil et al. [12] identified *SF3B1* mutations in six cases and in a subsequent large-scale mutation analysis, confirmed the high frequency of *SF3B1* mutations in MDS (72/354; 20 %), which were rare in other myeloid neoplasms, including AML (3/57; 5 %), CML (0/53), and MPNs (12/420, 3 %). Moreover, Yoshida et al. [13] analyzed 29 cases with different subtypes of myelodysplasia and identified mutations of multiple components of the RNA splicing machinery, including *SF3B1, U2AF35, SRSF2, ZRSR2, SF3A1* and *PRPF40B*, in 16 cases. Affecting at least eight components of the RNA splicing machinery, mutations were found in 130 of 228 MDS (57 %), 48 of 88 CMML (55 %) and 16 of 62 secondary AML (25.8 %) cases, but relatively rare in de novo AML (10/151; 6.6 %) and MPNs (5/53; 9.4 %) [13]. These observations were confirmed in subsequent studies [15–27], although splicing factor mutations seem to be rare in pediatric myeloid neoplasms, including juvenile myelomonocytic leukemia [28, 29].

Pathway mutations involving the RNA splicing machinery

RNA splicing provides a basic cellular mechanism for expression of genetic information [30]. Common to all eukaryotes, this mechanism allows for generating a large diversity of protein species in the face of limited set of genes by alternative splicing [31]. RNA splicing is accomplished by recruitment and disengagement of multiple snRNP complexes and other protein factors to newly transcribed pre-mRNA, through which exon–intron boundaries are recognized and intronic sequences were correctly spliced out to generate mature mRNA [30]. RNA splicing is initiated by the recognition of 5′ splice site by a U1 snRNP complex, followed by the recruitment of a complex consisting of a U2AF35/65 heterodimer, ZRSR2 and an SR protein such as SRSF1 or 2, and other factors to recognize the 3′ splice site. Finally, a U2 snRNP complex replaces SF1 bound to the branchpoint sequence with one of its subcomponent, SF3B1, to establish a splicing A complex (Fig. 1) [30, 32]. Notably, most of the mutated splicing factors in MDS belong to the A complex, occurring largely in a mutually exclusive manner, strongly indicating that the common functional target of these mutations should be the 3′ splice site recognition (Table 1) [13].

Presence of mutational hot spot in *SF3B1, SRSF2,* and *U2AF35*

Another conspicuous feature of splicing factor mutations is the presence of mutational hot spots in major mutational targets, including *SF3B1, SRSF2* and *U2AF35*. In *U2AF35*, the mutations almost exclusively involved highly conserved two amino acid positions, S34 and Q157, within the N- and C-terminal zinc finger domains, while almost all *SRSF2* mutations are missense changes at P95 or deletions involving this amino acid position [13, 17, 21, 23]. Less conspicuously, *SF3B1* mutations were confined to 5–7 amino acid positions within the domains corresponding to exons14–15, of which ~50 % of the mutations were accounted for the K700E [12, 13]. No homozygous mutations have been reported for these three genes. The presence of hot spots and the absence of nonsense or frameshift

Table 1 Splicing factor mutations in myeloid neoplasms

Gene	Chromosome	Size (aa)	Frequency	Phenotype association	Mutational hot spots	Functions
SF3B1	*2q33.1*	1304	Common	RARS, RCMD-RS	K700, K666, K662, K622	3′ recognition
SRSF2 (SC35)	*17q25.1*	221	Common	CMML	P95	3′ recognition
U2AF35 (U2AF1)	*21q22.3*	240	Common	MDS/CMML	S34, Q157	3′ recognition
ZRSR2	*Xp22.1*	483	Common	MDS/CMML	Nonsense, frameshift	3′ recognition
SF3A1	*22q12.2*	793	Rare	Unclear	None	3′ recognition
U2AF65 (U2AF2)	*19q13.42*	475	Rare	Unclear	None	3′ recognition
SF1	*11q13.1*	639	Rare	Unclear	None	3′ recognition
PRPF40B	*12q13.12*	871	Rare	Unclear	None	3′ recognition (speculated)
PRPF8	*17p13.3*	2335	Rare	Unclear	None	Aligning 5′ and 3′ exons
LUC7L2	*7q34*	392	Rare	Unclear	None	Recognition of nonconsensus splice sites

changes strongly suggested that they could be associated with some gain of function rather than represented simple loss of functions. In contrast, mutations of *ZRSR2* on X chromosome were distributed along the entire coding region [13]. About two-thirds of mutations were either nonsense or frameshift changes, causing a premature stop codon [13, 17, 23]. The majority of the *ZRSR2* mutated cases were male, in which single mutations resulted in complete loss of functions [13].

Genotype–phenotype association

While compromised 3′ splice site recognition seems to be a common consequence of different splicing factor mutations, there exist strong genotype and phenotype associations for splicing factor mutations. This is most prominent for the association of *SF3B1* mutations with increased ring sideroblasts. *SF3B1* mutations were found in 68–82 % of refractory anemia with ring sideroblasts (RSRS) and 57–76 % of refractory cytopenia with ring sideroblasts (RCMD-RS) [12, 13, 15, 18]. Malcovati et al. [33] reported that regardless of disease type, SF3B1 mutations strongly predicted the presence of increased sideroblasts with 97.7 % positive predictive value, although it did not necessarily satisfy the criteria for RARS or RCMD-RS (i.e., 15 % of all erythroblasts). Less prominently, *SRSF2* mutations were more frequently found in CMML (30.7–47 %) than in other subtypes of myeloid neoplasms [13, 21]. Interestingly, *SF3B1* mutations, but not other splicing factor mutations, have also been reported in 5–15 % of chronic lymphocytic leukemia (CLL), especially in high-risk cases [34–38]. In addition, *SF3B1* are mutated in several solid cancers, including breast, bladder, endometrial and other cancers, although the mutation frequencies were low [12, 39]. These genotype–phenotype associations may reflect gene-specific functions of individual mutations. For example, *SF3B1* was shown to participate in Hox gene regulation through functional interaction with *polycomb* and *trithorax* genes [40]. *SRSF2* has also been implicated in genetic stability, and its defect could lead to hypermutability [41].

Impact of spliceosome mutations on clinical outcome

Several reports have described the clinical impact of splicing factor mutations. However there appear to be discrepancies in this impact among different studies. Initial reports indicated a significantly better overall survival for *SF3B1* mutated cases compared to unmutated cases in MDS [12, 33], while other studies showed no significant impact of the mutations on survival [18, 23, 27]. *SRSF2* mutations were reported to be associated with poor prognosis in univariate analysis, but may not be an independent prognostic predictor [18, 23, 27]. Also, *U2AF35* mutations were associated with poor prognosis or higher risk of progression to AML in univariate analysis in some series [14, 42] but not in others. To elucidate the exact impacts of splicing factor mutations, a well-designed control study should be required taking other common mutations also into account.

Abnormal RNA splicing caused by splicing factor mutations

The high frequency of mutations in different components of the RNA splicing machinery in MDS suggests that

abnormal RNA splicing is the common consequence of these mutations, which is relevant to the pathogenesis of MDS. However, their effects on RNA splicing have been evaluated only in a very limited context. When expressed in HeLa cells, the S34F U2AF35 allele induces global defects of splicing, causing abnormal retention of intronic sequences in a wide variety of mature mRNA species [13]. On the other hand, the same mutation was shown to promote splicing and exon skipping of a minigene reporter in 293T cells [14]. These are observations in highly artificial systems; no information about abnormal splicing is available for other splicing factor mutants. To understand the role of these mutations in MDS pathogenesis, the effects of the mutant alleles on RNA splicing should be evaluated in more physiological conditions using primary hematopoietic cells. It is particularly important to identify the gene targets of possible splicing defects.

Biological impact of mutations

To date, biological consequences of splicing factor mutations have been tested only for *U2AF35* mutants. Unexpectedly, S34F U2AF35 mutant-transduced HeLa cells showed severely suppressed cell growth rather than enhanced cell proliferation, accompanied by apoptosis and G2/M arrest [13]. The effect of the S34F and Q157P/R U2AF35 mutants was also tested in competitive repopulation assays, in which highly purified mouse hematopoietic stem cells ($CD34^{-}c\text{-}Kit^{+}Scal^{+}Lin^{-}$) were transduced with each mutant and together with normal competitors, transplanted into lethally irradiated mice. In this assay, mutant transduced stem cells showed lower repopulating capacity compared to mock- or wild-type *U2AF35*-transduced cells, as determined by the chimerism in peripheral blood 6 weeks after transplantation [13], indicating that both *U2AF35* mutants could disturb normal hematopoiesis. However, the lower repopulation of mutant-transduced stem cells raises a serious difficulty to our understanding of how *U2AF35* mutated cells achieve clonal dominance over the remaining normal hematopoietic cells, although some oncogenes, such as oncogenic RAS, have been shown to induce apoptosis rather than transformation and promotion of cell growth depending on cell contexts [43, 44]. The importance of cooperation with coexisting mutations and/or the effects of abnormal bone marrow environment represent possible explanations.

Concluding remarks

Whole exome sequencing has revealed the otherwise unexpected involvement of multiple components of the RNA splicing machinery by gene mutations that characterize MDS and related myeloid neoplasms and as such, demonstrated the power of massively parallel sequencing technologies in cancer research. This discovery represents a significant advance in the field of MDS research, providing a novel clue to understanding of the pathogenesis of MDS. However, a number of critical issues remain unsolved: what is the molecular mechanism for these mutations to contribute to MDS pathogenesis, to what extent the deregulated RNA splicing could be involved in that process, what is the molecular nature of the predicted gain-of-functions, and what are the targets of these genes. Their impact on clinical parameters should also be clarified. Finally, the question of whether the recently characterized small molecular inhibitor of SF3B1 might have a therapeutic role in the treatment of myeloid neoplasms with splicing factor mutations remains to be addressed [45–47].

Acknowledgments This work was supported by Grants-in-Aid from the Ministry of Health, Labor and Welfare of Japan and KAKENHI (23249052, 22134006, and 21790907).

Conflict of interest None.

References

1. Corey SJ, Minden MD, Barber DL, Kantarjian H, Wang JC, Schimmer AD. Myelodysplastic syndromes: the complexity of stem-cell diseases. Nat Rev Cancer. 2007;7:118–29.
2. Bejar R, Levine R, Ebert BL. Unraveling the molecular pathophysiology of myelodysplastic syndromes. J Clin Oncol Off J Am Soc Clin Oncol. 2011;29:504–15.
3. Shih AH, Abdel-Wahab O, Patel JP, Levine RL. The role of mutations in epigenetic regulators in myeloid malignancies. Nat Rev Cancer. 2012;12:599–612.
4. Levine RL, Carroll M. A common genetic mechanism in malignant bone marrow diseases. New Engl Journal Med. 2009;360:2355–7.
5. Delhommeau F, Dupont S, Della Valle V, James C, Trannoy S, Masse A, et al. Mutation in TET2 in myeloid cancers. New Engl J Med. 2009;360:2289–301.
6. Ley TJ, Ding L, Walter MJ, McLellan MD, Lamprecht T, Larson DE, et al. DNMT3A mutations in acute myeloid leukemia. New Engl J Med. 2010;363:2424–33.
7. Mardis ER, Ding L, Dooling DJ, Larson DE, McLellan MD, Chen K, et al. Recurring mutations found by sequencing an acute myeloid leukemia genome. New Engl J Med. 2009;361:1058–66.
8. Langemeijer SM, Kuiper RP, Berends M, Knops R, Aslanyan MG, Massop M, et al. Acquired mutations in TET2 are common in myelodysplastic syndromes. Nat Genet. 2009;41:838–42.
9. Yan XJ, Xu J, Gu ZH, Pan CM, Lu G, Shen Y, et al. Exome sequencing identifies somatic mutations of DNA methyltransferase gene DNMT3A in acute monocytic leukemia. Nat Genet. 2011;43:309–15.
10. Bejar R, Stevenson K, Abdel-Wahab O, Galili N, Nilsson B, Garcia-Manero G, et al. Clinical effect of point mutations in myelodysplastic syndromes. New Engl J Med. 2011;364:2496–506.